Climatic Influence on Sediment Distribution and Transport in the Thar Desert (Sindh and Cholistan, Pakistan)

Muhammad Usman[1*], Peter D. Clift[2,3*], Guido Pastore[1], Giovanni Vezzoli[1], Sergio Andò[1], Marta Barbarano[1], Pieter Vermeesch[2], Eduardo Garzanti[1]

[1]Laboratory for Provenance Studies, Department of Earth and Environmental Sciences, University of Milano-Bicocca, Milano 20126, Italy

[2]London Geochronology Centre, Department of Earth Sciences, University College London, London C1E 6BT, UK

[3]Department of Geology and Geophysics, Louisiana State University, Baton Rouge, LA 70803, USA

*Corresponding Authors: musman1@campus.unimib.it, pclift@lsu.edu

Abstract

The Thar Desert is a major sediment depocenter in southwestern Asia and borders the Indus drainage system to its east. It is unclear where the sediment that built the desert is coming from, and when the desert experienced phases of construction. In particular, we seek to establish the role of the South Asian monsoon in the initial formation and subsequent expansion of the desert. Here we integrate bulk-petrography and heavy-mineral data with U-Pb ages of detrital-zircon, to understand how the desert relates to the major potential sediment sources in the Himalayan orogen and to the major rivers that surround it. Bulk petrography and heavy mineral data from eolian sand in Cholistan (NE Pakistan) show close similarity with that of Himalayan tributaries, whereas eolian sand in Sindh (S Pakistan) contains heavy-mineral suites close to those of Indus sand largely supplied by erosion of the Karakorum and Kohistan.

Kohistan is a particularly rich source of heavy minerals and is thus over-represented in sediment budgets based on that proxy alone. U-Pb ages of detrital-zircon fail to show a sharp difference between dune sands in Sindh and Cholistan, except for revealing somewhat greater supply from the Himalaya in Cholistan and from the Karakorum, Kohistan and Nanga Parbat in Sindh. Zircon ages are similar in Sindh desert sand and in the Indus Delta and are most similar in deltaic sand dated as 7 ka or older. In parallel, the age signature of Cholistan sands resembles more that of older river channels found along the northwestern edge of the desert (e.g., paleo-Ghaggar-Hakra) than that of modern Himalayan tributaries (e.g., Sutlej). Both Cholistan and Sindh sands suggest that sediment supply to the desert was greater in the early Holocene when the monsoon was stronger. The southwesterly summer monsoon turned out to be the most effective agent of eolian transport and recycling of Indus delta sediments entrained towards the central and northern parts of the desert.

Key words: Provenance analysis; sand petrography; heavy minerals; detrital-zircon geochronology; Climate change; Thar Desert.

1. Introduction

Source-to-sink studies in major siliciclastic sedimentary systems, especially those supplied by rivers from major mountain belts is complicated by the buffering processes involved with eolian sand seas. Large volumes of sediment may be stored and then recycled as a river system passes across or nearby a sandy desert area on its way to the final depocenter. Changing paleoenvironmental conditions may exercise an important control on how sediment is transported across or recycled within desert areas. Changing amounts and seasonality of precipitation may have an important impact on the growth or reduction of desert sand areas and on their impact on the associated rivers. The fraction of sandy sediments deflated from the river channel and floodplain and stored in the sand sea is referred to as the net sediment loss from the source system (Trimble, 1983; Petter et al., 2013). These stored sediments may be subsequently eroded and mixed with additional fluvial sediment within the drainage basin. Buffering and recycling of sediment in this way may disrupt the propagation of erosional signals related to climatic change or tectonic events (Whipple, 2001; Alizai et al., 2011a; East et al., 2015; Garzanti et al., 2022).

Our ability to resolve the factors that control fluvial-aeolian interactions is affected by mixing of new and recycled sediment within the basin. In this study, we aim to better quantify the processes that control sediment storage and recycling in the western Thar Desert, fed by the Indus River and its Punjab tributaries draining together the Tibetan Plateau and the Karakorum and western Himalayas ranges. Understanding how this sediment-filtering system works represents an essential step to enhance our ability to interpret the more continuous deep-marine depositional record in the Arabian Sea.

The efficiency of sediment supply to the Thar Desert on long timescales (>10^4 y) is controlled by the interaction between monsoonal climate and rock uplift in the active mountain belts of the Himalaya and Karakorum. This huge sedimentary system is a suitable region for studying this type of source-to-sink problem, characterized by the intensity of the Southwest monsoon and the strong tectonic activity of orogenic sources, which provide clear signals in the sediment carried to the lower reaches of the Indus River. The Himalaya-Karakorum-Tibet orogen is the result of ongoing collision between the Indian and Eurasian continental masses since ~60 Ma (Critelli et al., 1994; Garzanti et al., 1996; Guillot et al., 2003; Hu et al., 2015; Najman et al., 2003, 2017). Ongoing tectonically-driven rock uplift coupled with rapid incision is responsible for the extreme high relief and rapid exhumation characterizing the western Himalayan syntaxis drained by the Indus River (Zeitler et al., 1993; Garzanti et al., 2020a, b).

If we are to understand the tectonics and erosion of this mountain belt over million-year timescales, then this can only be achieved using the Indus River and its associated sedimentary archive, because the record of past exhumation has been removed from the source ranges by erosion. In contrast, the sediment record in the Arabian Sea and Himalayan foreland basin can be used to reconstruct changing patterns and rates of erosion through provenance studies of the detrital sediment flux from the orogenic region (Clift et al., 2001; Clift et al., 2008; Clift and Jonell, 2021). In recent times, all sediment flowing from the various sources into the ocean basin has passed next to or through the Thar Desert, but the processes that operate in this region are not well studied and poorly understood.

Studies of sediments in arid and semi-arid regions seldom pay sufficient attention to the interactions that occur during fluvial and aeolian transport (e.g., Thomas and Wiggs, 2008; Belnap et al., 2011; Feder et al. 2018; Liang et al., 2023). These are likely to introduce complexities to the original erosional pulse that might be linked to environmental change, and whose compositional signature closely reflects the eroded source rocks. In the case of the Indus River system, such a change mainly occurs in the Thar Desert, extending across SE Pakistan and NW India (Figs. 1 and 2). In the Thar Desert, the complex nature of sediment transport and recycling has not so far been adequately investigated, even though a better understanding of these processes are essential to constrain the ongoing fluvial-eolian interactions during source-to-sink transport. The sediments stored in the desert reflect the net effects of sediment transport from hillslope to alluvial channels and finally to the dryland area (Ramsey et al., 1999; Prins et al., 2009; Bracken et al., 2015). This transport may be modulated by changes in the environment, as well as in the development of the drainage system that may be particularly influenced by tectonic activity. The arid-semi arid Thar Desert is quite sensitive to fluvial activity and changing climate. The fluvially supplied eolian sands are stored in the dune field and reworked by winds. Subsequently, the sediments may interact further with the river and continue their journey to the ocean (Bullard and Livingstone, 2002; Bullard and McTainsh, 2003; Alizai et al., 2011b). Wind is a strong transforming agent that can move sediments hundreds of kilometers from the original fluvial source (Langford, 1989; Garzanti et al., 2017) until they are eventually stored in dune fields such as the Thar Desert.

Climate change affects summer-monsoon winds, which move sediment from southwest to northeast across the Thar Desert (Wasson et al., 1983; Singhvi and Kar, 2004; East et al., 2015). This summer transport path is reversed in winter, but this system only plays a marginal role in sand transport, whereas dust storms are associated with early summer monsoon rain in the southwestern Indian subcontinent (Singhvi et al., 2010). The principal aim of the present study is to improve our understanding of the influence that climate change exerts on sediment transport towards and across the Thar Desert by using bulk-petrography, heavy-minerals, and detrital-zircon U-Pb age analyses to trace sediment transport pathways. We reconstruct how sediments were fed into and distributed within the Thar Desert in recent times and evaluate the impact of Holocene environmental and climatic changes on sediment generation in the western part of the Himalayan orogen.

2. Thar Desert

2.1. Geomorphological framework

The term "desert" passed from the Egyptian hieroglyphics *Tésert* to the Latin word *desertum* (place of abandoned wilderness) to describe rainless dune field areas (El-Baz, 1983). El-Baz (1983) argued that a desert is "*a vast area of dune fields and arid land where wind blows dust in the air and moves sand grains across dune profiles*". Dune sediments are easily eroded and deflated by wind action. Sand derived from mountain sources is thus affected by repeated reworking and recycling during fluvial-eolian interactions.

The Thar Desert, situated in the western Indian subcontinent in an arid environment of sandy rolling hills (locally named "*thul*"), covers ~200,000 km^2 including the Punjab and Sindh provinces in Pakistan, and the Gujarat and Rajasthan states in India. Sand dunes stretch from north to south for ~800 km and merge in the west into the fertile alluvial plains of the Indus River in Pakistan. The southern side of the desert is bound by the foothills of the NNE to SSW-trending Proterozoic Aravalli ranges in Gujarat (Kar, 2013). The Pakistani part of the Thar Desert includes the Cholistan Desert in the north (Bahawalpur district, Punjab) and the Sindh Desert in the south (Sindh Province). Thar Dunes are remarkable for their constant movement by wind erosion and deposition (Sam et al., 2015), which prevents permanent human settlement (Nordstrom, 2014).

The Cholistan Desert, ~480 km in length and between ~23 and ~192 km in width, covers an area of ~26,000 km^2 (Figs. 1 and 2). Two regions are distinguished based on geomorphological differences, Lesser Cholistan (12,370 km^2) and Greater Cholistan (13,960 km^2) (Akhtar and Arshad, 2006; Ahmed, 2011). Lesser Cholistan at the northern edge of the desert comprises low dune ridges and alluvial flats (Akbar et al., 1996; Mughal, 1997; Mughal et al., 2016) and lies around the Ghaggar-Hakra paleochannel which is a now abandoned Himalayan-sourced Punjabi tributary flowing closest to the desert and that contains remnants of sandy fluvial terraces (Ahmad, 2008) and may have formerly joined the Nara River to the south of Cholistan (Clift et al., 2012; Srivastava et al., 2020). Greater Cholistan in the south is dominated by sand dunes. The Sindh Desert, ~500 km in length and between ~38 km and ~200 km in width, covers an area of ~45,790 km^2 characterized by undulating sand ridges (Chauhan, 2003) (Figs. 1 and 2).

2.2. Thar Desert climate and the Monsoon

The geographic position of the Thar Desert, surrounded by mountain ranges, rivers and alluvial plains, contributes significantly to the weather patterns that shape its distinctive, hot and dry environment. Seasonal winds from the Indian Ocean lose moisture as they approach the Himalayan front where most of the precipitation is released, and a low-pressure system develops adjacent to the mountains in the summer by trapping hot air over the plains (Wang et al., 2005; Boos and Kuang, 2010). The Thar Desert region, which lies on the western edge of this circulation system and is also affected by dry westerly winds from the arid Makran Desert and Afghanistan, has consequently very low precipitation throughout the year (100–200 mm/a; Akbar et al., 1996; Rahaman et al., 2009). Furthermore, the Thar Desert lies in the rain shadow of the Aravalli Range, which contributes to its aridity, with high temperatures that cause strong evaporation (Kumari et al., 2023).

All rain carried by monsoon clouds is absorbed by surrounding regions, so that monsoon winds in the Thar Desert are hot and dry. Nevertheless, the Asian Monsoon remains crucial to the Thar Desert region, delivering 90% of rainfall in Cholistan (100–500 mm/a) during the summer months (May to September, Bookhagen, 2010). The weaker winter monsoon provides little additional precipitation, but some rainfall in the northern part of the desert is associated with winter westerlies. The Thar Desert in Sindh receives ~100 mm of rain in the west and ~500 mm in the east, with significant variations from year to year. The hottest months (temperatures up to 50°C) are May and June, whereas the coldest month is January when frost is frequent (mean minimum temperature 5°–10°C). Dust storms and dust-raising winds with velocities up to 145 km/h are common in May to June.

The Asian Monsoon responds linearly to orbital forcing during obliquity (41 k.y.) and precession (23 k.y.) cycles (Prell, 1984; Clemens et al., 1996; Clemens and Prell, 2003).

Monsoon intensity is affected by changes in the volume of Arctic and Antarctic icecaps, and by temperatures in both northern and southern hemisphere resulting from cross-equatorial exchanges of atmospheric heat and pressure (Blinkhorn, 2014). Maximum monsoonal intensity is observed during glacial minima, whereas a steep inter-polar temperature gradient commonly produces a monsoonal minimum ~20 k.y. before the glacial maximum (Zhisheng et al., 2011). Paleoenvironmental data suggest that the Thar Desert may have experienced reduced monsoonal rainfall between ~40 ka and ~20 ka.

2.3. Paleochannels and sediment flux

The western Himalayan foreland flood plains have been re-incised by the Indus River since ~10 ka, following earlier aggradation during deglaciation (Giosan et al., 2012). Fluvial discharge was mainly controlled by regional monsoonal precipitation, as well as by melting of snow and ice in the Himalayan-Karakorum headwaters (Bookhagen, 2010; Durcan et al., 2010). Several major tributaries supply sediment from orogenic sources to the Indus lower reaches, including the Shyok, Shigar, Gilgit and Kabul tributaries of the upper Indus and the five Punjab (*punj*, five; *ab*, water) tributaries (Jhelum, Chenab, Ravi, Beas, and Sutlej) of the lower Indus (Fig. 1).

The mainstream of the Indus River rises from glaciers north of Mt. Kailas and flows for a third of its course along the Indus suture zone before cutting southwards across the Western Himalayan Syntaxis, eventually meeting the Himalayan front where it is now barred by the Tarbela Dam (Fig. 1). The Punjab tributaries cut across the entire Himalayan belt and account for ~44% of total Indus discharge (Alizai et al., 2011a).

The Indus River has undergone several drainage changes through time. Western migration of the river courses has occurred in Sindh since the Last Glacial Maximum (LGM) (Kazmi, 1984). Other major recent changes include the loss of the Yamuna River, captured by the Ganga River between 10 and 50 ka, and the drying up of the Ghaggar-Hakra tributary (Valdiya, 2002; Saini et al., 2009; Clift et al. 2012; Giosan et al., 2012). The Punjabi tributaries have also experienced repeated changes (Amundson et al., 1986; Wright et al., 2005): the Sutlej River lost contributions from the Yamuna River before 17 ka (Stein, 1942; Sinha et al., 2013; Sinha et al., 2019) and the Ravi drainage moved northwards in the middle Holocene.

Tentative estimates indicated that ~11% of the sediment reaching the Arabian Sea in the Holocene was supplied by incision into the northern floodplains, and another ~6% by recycling of Thar Desert sands (Clift and Jonell, 2021). Reworking of Thar Desert sediment occurred after 10 ka, when the Indus and its tributaries incised into the lower reaches of the western Punjabi floodplains (Giosan et al., 2012). Sediment deposited in the Thar Desert date from at least mid-Pleistocene time (Glennie et al., 2002; Singhvi et al., 2010) and 173 ka-old fluvial channels have been identified in the central part of the Thar Desert (Blinkhorn et al., 2020). More recent fluvial channels around the western edge of the desert were abandoned at ~4–5 ka and were buried under parabolic dunes at ~1.4 ka (Clift et al., 2012). Younger intermittent fluvial activity at 2.9–0.7 ka has also been reported from both the upper and lower Ghaggar-Hakra floodplain (Giosan et al., 2012). Evidence from Pb-isotope studies of detrital K-feldspar (Alizai et al., 2011b) and chemistry of detrital garnet (Alizai et al., 2016) in the Nara Valley suggested that the Nara River was either a former course of the river Indus or an ephemeral stream entirely fed with reworked sediments.

2.4. Climatic changes

Because climatic changes have a strong influence on sediment generation and fluvial transport (Haughton, 1991; Gábris, and Nádor, 2007), the study of alluvial deposits offers a key to paleoclimatic reconstructions (Van de kamp and Leake, 1985; Velbel and Saad, 1991). The present arid climate of the Thar Desert was established at ~4 ka, after a wet middle Holocene stage preceded by dry conditions in the early Holocene (Dhir and Singhvi, 2012). Luminescence ages indicate relatively inefficient aeolian sediment transport during the LGM (Singhvi and Kar, 2004; Singhvi et al., 2022). In contrast, stronger summer monsoonal winds increased aeolian transport during the Holocene, where sediment supplied during times of heavier rain was blown into the central part of the Thar Desert, where it rapidly accumulated throughout the Holocene (Singhvi et al., 2010; Chatterjee and Ray, 2017). Dunes along the western edge of the desert have advanced over the floodplains only more recently, and the connectivity between the Indus River and Thar dune fields has been documented by stratigraphic studies indicating eolian sediment transport mostly from the southwest (East et al., 2015). This general pattern is consistent with sediment mineralogy, and optically stimulated luminescence (OSL) and thermoluminescence (TL) ages (Singhvi et al., 2010). The Thar Desert expanded after the LGM, during phases of strengthened summer monsoon, and continued to advance westward during weakening of the summer monsoon starting after 8 ka. Pb isotope compositions of detrital K-feldspar grains, along with U-Pb zircon and Nd isotopic data, highlight a similarity between the lower reaches of the Indus River and the northern Cholistan Desert (Alizai et al., 2011a, 2011b).

3. Geological setting of the Thar Desert

Quaternary sediments of the Thar Desert, interspersed with low hills where Cenozoic rocks are locally exposed, are underlain by Archean gneiss, non-conformably covered by Proterozoic sedimentary rocks (~2.5 Ga to 541 Ma) and more recent alluvium (Roy and Smykatz-Kloss, 2007; Jain and Banerjee, 2020). Desert sediments of original fluvial origin were repeatedly deflated by wind into sand ridges, even including clay locally. Sand in the northern Cholistan Desert is largely derived from the Himalaya and supplied from the Sutlej River (Ahmed, 2008).

Sand in the southern Sindh Desert, instead, is mainly sourced from the Indus River largely sourced from the Karakorum Range and the Kohistan Arc, as well as the Himalaya and representing the main source for sediments fed into the Arabian Sea (Clift et al., 2002; Garzanti et al., 2020a)

The main potential sediment sources to the Indus River and Thar Desert are the Karakorum and Hindukush, the Western Himalayan Syntaxis (WHS, i.e., Nanga Parbat Massif), Transhimalayan arcs (Henderson et al., 2010), the NW Greater and Lesser Himalaya, and subordinately the ranges bounding Pakistan to the west, i.e., Kirthar and Sulaiman ranges (Guillot et al., 2003; Garzanti, 2019a). The Kohistan and Ladakh arcs are bound by the Shyok and Indus Sutures to their north and south (Debon et al., 1987; Garzanti and Haver, 1988; Treloar et al., 1996; Rolland et al., 2000). The Nanga Parbat Massif is cut by the Indus River but supplies a notably lower amount of sediment than the eastern syntaxis despite its rapid exhumation (Clift et al., 2022). The main focus of erosion are the Karakorum domes (Lemennicier et al., 1996; Crawford and Searle, 1992; Searle et al., 1999; Rolland et al., 2001; Searle et al., 2010) cut by the Hushe, Braldu and Hispar rivers (Garzanti et al, 2020b).

4. Fingerprinting sand sources

Sand in the Thar and Thal deserts is supplied by the Upper Indus that drains the Ladakh and Kohistan arcs, the Karakorum and Hindukush ranges, the Nanga Parbat Massif, and the Punjabi tributaries (Jhelum, Chenab, Ravi, Beas, and Sutlej) draining the Himalaya (Liang et al., 2019; Garzanti et al., 2020b).

The Ladakh Arc supplies quartzo-feldspathic to feldspar-rich feldspatho-quartzose, plutoniclastic sand with a rich to very rich transparent heavy mineral (tHM) suite dominated by amphibole (mostly hornblende) with epidote and minor clinopyroxene (mainly diopside) and titanite.

The Kohistan Arc supplies feldspatho-quartzo-lithic to litho-quartzo-feldspathic metamorphiclastic sand with common prasinite and epidote-amphibolite grains (Garzanti et al., 2005). The very rich to extremely rich tHM suite is dominated by amphibole (mainly hornblende or pargasite associated with actinolite or hastingsite) with common epidote-group minerals (mostly clinozoisite) and pyroxenes (diopside, pigeonite, augite, and hypersthene).

The Karakorum supplies quartzo-feldspatho-lithic (North Karakorum) to quartzo-feldspathic plutoniclastic (Central Karakorum), and litho-feldspatho-quartzose metamorphiclastic sand with marble grains (South Karakorum). Mainly moderately rich tHM suites include common amphibole (mainly hornblende with pargasite, hastingstite, or actinolite), epidote-group minerals (epidote, clinozoisite, and allanite), garnet mostly derived from intermediate-acidic igneous rocks (Bi-type, following Mange and Morton, 2007), titanite, common diopsidic clinopyroxene, and minor kyanite, staurolite, and sillimanite.

The Zanskar River draining the northern side of the Greater Himalaya which contribute litho-feldspatho-quartzose metamorphiclastic sand, with a moderately rich tHM suite including amphibole (pargasite and hornblende with minor hastingsite), mostly Bi-type garnet, fibrolitic sillimanite, kyanite, epidote-group minerals (epidote, clinozoisite, minor allanite), and pyroxenes (diopside, augite, and locally hypersthene). The Nanga Parbat Massif contributes feldspar-rich feldspatho-quartzose sand with a very rich tHM suite dominated by amphibole (mainly hornblende with common tschermakite and minor pargasite) with clinopyroxene (diopside with rare augite), garnet mainly derived from high-grade metabasic rocks (Ci-type) and minor from amphibolite-facies metasediments (Bii-type) (Mange and Morton, 2007), epidote, clinozoisite, and sillimanite.

Cenozoic foreland basin sedimentary strata are incised by the Soan River and shed feldspatho-litho-quartzose sand with a moderately rich, epidote-dominated tHM suite with garnet, hornblende, and tourmaline.

5. Methods

For this study we collected 50 sand samples from the Sindh province in the southern Thar Desert and 40 sand samples from the Cholistan province in the northern Thar Desert (Fig. 1). Complete information on sampling sites is given in Appendix A Table A1 and in the Google Earth™ file Thar.kmz. The complete petrographic, heavy-mineral, and geochronological datasets are provided in Appendix A and B.

5.1. Sand petrography

A quartered fraction of each sand sample was impregnated with araldite epoxy and cut into a standard thin section stained with alizarine red to distinguish dolomite and calcite. Petrographic analysis was carried out by counting ~450 points under the microscope following the Gazzi-Dickinson method (Ingersoll et al., 1984). Sand classification was based on the relative abundance of the three main framework components quartz (Q), feldspars (F) and lithic fragments (L), considered if exceeding 10%QFL (e.g., a sand is named feldspatho-litho-quartzose if Q > L > F > 10%QFL or quartzo-lithic if L > Q > 10%QFL > F; classification scheme after Garzanti, 2019b). Metamorphic grains were classified according to their protolith and metamorphic rank, expressed by the metamorphic indices MI and MI* (Garzanti and Vezzoli, 2003). MI varies from 0 (detritus shed by sedimentary and volcanic cover rocks exclusively) to 500 (very-high-rank detritus exclusively shed by high-grade basement rocks). MI* considers only metamorphic rock fragments and thus varies from 100 (very-low-rank detritus shed by very low-grade metamorphic rocks) to 500. Petrographic parameters used in this article include the plagioclase/total feldspar (P/F) ratio; feldspar with cross-hatch twinning is referred to as microcline. Median grain size was determined in thin section by ranking and visual comparison with in-house standards of sieved Φ/4 classes. Significant detrital components are listed in order of abundance (high to low) throughout the text. Key compositional parameters are summarized in Table 1 and the complete dataset is provided Appendix A, Table A2.

.

5.2. Heavy minerals

From a split aliquot of the 15–500 µm size window obtained by wet sieving, heavy minerals were separated by centrifuging in Na-polytungstate (2.90 g/cm^3), and these were then recovered by partial freezing with liquid nitrogen (Andò, 2020). For each sample, ~250 transparent heavy minerals (or all of those present in the grain mount) were point-counted at appropriate regular spacing to minimize overestimation of smaller grains. Transparent heavy-mineral assemblages, called for brevity "tHM suites" throughout the text, do not include alterites, phyllosilicates and carbonates (Garzanti and Andò, 2019). According to the transparent-heavy-mineral concentration in each sample (tHMC), tHM suites are defined as extremely poor (tHMC < 0.1), very poor ($0.1 \leq$ tHMC < 0.5), poor ($0.5 \leq$ tHMC <1), moderately poor ($1 \leq$ tHMC <2), moderately rich ($2 \leq$ tHMC <5), rich ($5 \leq$ tHMC < 10), or very rich (tHMC > 10). The sum of zircon, tourmaline, and rutile over total transparent heavy minerals (ZTR index of Hubert, 1962) measures the relative proportion of durable minerals in the tHM suite and can thus be considered as an index of recycling (Garzanti, 2017). Key heavy-mineral parameters are summarized in Table 1 and the complete dataset is provided Appendix A, Table A3.

5.3. Detrital-zircon geochronology

Starting from the heavy-mineral separates of five samples (two from the Cholistan Desert and three from the Sindh Desert), zircon grains were concentrated with standard magnetic techniques, directly mounted in epoxy resin without any operator selection by hand picking, and identified by automated phase mapping (Vermeesch et al., 2017) under a Renishaw inVia™ Raman microscope. U-Pb zircon ages were determined at the London Geochronology Centre using an Agilent 77003 LA-ICP-MS system, employing a NewWave NWR193 Excimer Laser operated at 10 Hz with a 25-lm spot size and ~ 2.5 J/cm^2 fluence. No cathodoluminescence imaging was done, and the laser spot was always placed blindly in the middle of zircon grains to treat all samples equally and avoid bias in inter sample comparison ('blind-dating strategy' as discussed in Garzanti et al., 2018). The mass spectrometer data were converted to isotopic ratios using GLITTER 4.4.2 software (Griffin et al., 2008), employing Plešovice zircon (Sláma et al., 2008) as a primary age standard and GJ-1 (Jackson et al., 2004) and 91500 (Wiedenbeck et al., 1995) as a secondary age standard (Appendix B, Figs. S1 and S2). A NIST SRM612 glass was used as a compositional standard for U and Th concentrations. GLITTER files were post-processed using IsoplotR (Vermeesch et al., 2018). Concordia ages were calculated as the maximum likelihood intersection between the concordia line and the error ellipse of $^{207}Pb/^{235}U$ and $^{206}Pb/^{238}U$ (Ludwig, 1998). The discordance cutoff was set at –5/+15 of the concordia distance (Vermeesch, 2021). Concordant ages are provided in Appendix A Table A4.

5.4. Graphical/statistical tools

To visualize heavy-mineral data we use the compositional biplot (Gabriel, 1971), drawn using CoDaPack software (Comas-Cufí and Thió-Henestrosa, 2011). The biplot allows discrimination between multivariate observations (points) while shedding light on the mutual relationships among variables (rays). The length of each ray is proportional to the variance of the corresponding variable in the dataset. If the angle between two rays is close to 0°, 90° or

180°, then the corresponding variables are correlated, uncorrelated, or inversely correlated, respectively.

Statistical tools applied to U-Pb detrital-zircon age populations include multidimensional scaling (MDS; Kruskal and Wish, 1978; Vermeesch, 2013). MDS produces a map of points in which the distance between samples is approximately proportional to the Kolmogorov-Smirnov dissimilarity of their compositional or chronological signatures. Closest and second closest neighbors are linked by solid and dashed lines, respectively, and the goodness of fit is evaluated using the "stress" value of the configuration (0.2 = poor; 0.1 = fair; 0.05 = good; Vermeesch, 2013, 2018).

6. Compositional fingerprints and provenance of Thar Desert sands

6.1. Petrography and Heavy minerals

Cholistan Desert dune sand is feldspatho-litho-quartzose with dominant monocrystalline quartz and subequal plagioclase and K-feldspar (Figs. 3 and 4). Quartz content decreases southward from ~70% to ~57% (Table 1). The varied rock-fragment population consists of metasedimentary (paragneiss, schist, slate, calcschist, phyllite, metasandstone), metabasite (prasinite, chloritoschist, amphibolite), carbonate (limestone, dolostone), other sedimentary (shale, siltstone, minor chert), granitoid, felsic to mafic volcanic and metavolcanic, and minor ultramafic (serpentine schist, cellular serpentinite) grains (MI 256–326, MI* 239–314) (Figs. 3 and 4). Metamorphic and sedimentary lithics and the MI index tend to decrease SE-ward. Muscovite and biotite flakes are observed. The rich tHM suite includes hornblende, subordinate epidote and garnet, and minor clinopyroxene, hypersthene, staurolite, titanite, kyanite, and fibrolitic sillimanite (ZTR ≤ 4).

Sindh Desert dune sands are litho-felshpatho-quartzose, with plagioclase ≥ K-feldspar (P/F 49-60) (Figs. 3 and 4). Sedimentary rock fragments prevail over metapelite, metapsammite, and metavolcanic grains (MI 263–220). The rich tHM suite consists of blue/green to brown hornblende, subordinate garnet and epidote, minor clinopyroxene and hypersthene, sillimanite, kyanite apatite, and titanite (ZTR ≤ 3).

Sindh sand has less quartz than that from Cholistan (53± 2 *vs.* 60±2), more sedimentary than metamorphic lithics (Lm 39±6 Ls 58±5 *vs.* Lm 62±2 Ls 37±2), and higher heavy-mineral concentrations with overall similar amphibole-epidote-garnet tHM population typical of orogenic sediments (Garzanti and Andò, 2007; Fig. 4). This indicates a strong affinity to Indus River sand, especially in the southern part of the Sindh Desert, whereas samples from the Cholistan Desert have a greater affinity with sand transported by Punjabi tributaries sourced in the Himalaya.

6.2. Detrital-zircon geochronology

Data obtained in this study on dune sands from Cholistan (191 ages from 2 samples) and Sindh (330 ages from 3 samples), together with literature data from another three samples (East et al., 2015), compose a data set of 841 concordant ages overall (Table 2).

Zircon grains from Cholistan dunes yielded mainly Paleoproterozoic (26%) and Neoproterozoic (25%) ages (Fig. 5), with minor Neoarchean (2%), Mesoproterozoic (5%), Paleozoic (8%), Triassic (1%), Early Cretaceous (10%), Late Cretaceous (5%), Paleocene (5%), Eocene-Oligocene (9%) and Miocene (2%) ages (Appendix A Table A5).

Zircon grains from Sindh dunes are mainly Neoproterozoic ages (28%) and Paleoproterozoic (24%) ages, with significant Ordovician, Silurian, and Carboniferous ages (14% overall). Neoarchean (1%), Mesoproterozoic (7%), Triassic (1%), Jurassic (1%), Early Cretaceous (9%), Late Cretaceous (3%), Paleocene (6%), Eocene-Oligocene (4%), and Miocene (3%) ages also occur (Appendix A Table A5).

The youngest grains found both in Cholistan (13–21 Ma) and Sindh (17–25 Ma) are only known elsewhere in sand from the Hushe River draining the Baltoro Granite, and thus point to a provenance from the Karakorum Range (MDS, Fig. 6). Cretaceous to Oligocene grains are inferred to be predominantly derived from the Karakorum (characteristic peaks at 99–130 Ma and 24–43 Ma) and Transhimalayan arcs (43–96 Ma). Paleozoic and Neoproterozoic grains, most abundant in Sindh, are contributed by both Karakorum and Himalayan sources, whereas Mesoproterozoic to Paleoproterozoic (equally abundant in Cholistan and Sindh) are largely derived from the Greater Himalaya, Lesser Himalaya, and/or the Nanga Parbat Massif (Figs. 6 and 7).

7. Provenance budgets

The relative contributions from each geological domain to the aeolian sand of the Thar Desert can be estimated by forward mixing models (Garzanti et al., 2012; Resentini et al., 2017). Calculations, however, are nonunique and uncertain, influenced by potentially inaccurate compositional information on end-member sources and unverified assumptions. To ensure robust results, independent tests must be conducted using different criteria (Garzanti et al., 2020).

7.1. Petrography and Heavy minerals

Forward mixing calculations indicate that Indus River sand upstream of Tarbela Dam is derived ~60% from the Karakorum, ~20% from Transhimalayan arcs, ~13% from the Nanga Parbat massif, and ~6% from the Tethyan and Greater Himalaya (Garzanti et al., 2005; 2020) (Fig. 8a). These proportions change notably in the Lower Indus River, where sand is calculated to be derived 27±3% from the Karakorum, 10±3% from the Hindukush, 3±2% from the Ladakh Arc and Tibetan Plateau, 7±2% from the Kohistan Arc, 6±3% from the Nanga Parbat Massif, and 39±4% from the Himalaya, delivered largely by Punjab tributaries (Garzanti et al., 2005) (Fig. 8b).

Based on the integrated petrographic-heavy mineral dataset, dune sand in Cholistan is calculated to be derived ~30% from the Ladakh-Kohistan arcs, ~5% from the Karakorum–Hindukush ranges, ~17% from the Nanga Parbat Massif, and ~48% from Himalayan units (Fig. 8d). Instead, dune sand in Sindh is calculated to be derived ~34% from the Ladakh-Kohistan arcs, ~31% from the Karakorum–Hindukush ranges, ~16% from the Nanga Parbat Massif, and ~19% from Himalayan units (Fig. 8c).

Calculations based on petrographic data suggest that Cholistan sand dunes are mostly (up to ~90%) derived from Punjabi tributaries and dominantly from the Sutlej River flowing along the northern border of the Thar Desert (Fig. 8e). Calculations based on heavy-mineral data, however, indicate a major contribution (up to two thirds) from the Indus River (Fig. 8f). Some sediment may have been supplied also by the Ghaggar-Hakra River, formerly potentially connected with the Nara River in Sindh and for which we could not determine an end-member composition.

7.2. Detrital zircon ages

A set of forward mixing calculations based on the age populations illustrated above were performed using the *DZMix* software of Sundell and Saylor (2017). In each case, 10,000 attempts were made to match the observed zircon-age spectrum and the best 1% were selected. The best fit was separately assessed for Cholistan and Sindh samples using three statistical approaches (i.e., cross correlation, Kuiper test, and K-S test). End-members for source regions were characterized using detrital-zircon data from modern river sediments rather than bedrock data, because only the former provide a more representative weighed regional average of source-rock compositions. We use data from Zhuang et al. (2018) and Clift et al. (2022) for the Karakorum and Hindukush ranges, from Garzanti et al. (2020b) and Clift et al. (2022) for the

Nanga Parbat Massif, from Zhuang et al. (2018) and Garzanti et al. (2020b) for the Kohistan Arc, from Garzanti et al. (2020b) and Clift et al. (2022) for the Ladakh Arc, from Jonell et al. (2017) and Garzanti et al. (2020) for the Greater Himalaya, and from Alizai et al. (2011b) for Punjabi tributaries sourced in the Himalaya, separately considering data from the Sutlej and Beas Rivers that flow closest to the Cholistan Desert. As well as looking at modern Thar desert dunes, we also applied the same mixing calculations to the Upper Indus at Attock bridge (Alizai et al., 2011b; Garzanti et al., 2020b; Clift et al., 2022), and the modern lowermost Indus River at Thatta (Clift et al., 2004). We also considered data from post-LGM sediments of the Indus Delta and from older Cholistan sediments cored in the Marot borehole Clift et al. (2012).

The results of forward mixing calculations, provided in Appendix A Table A6 and in Figure 9a-h, with the latter showing the preferred contributions based on the V factor of the Kuiper test, indicate that zircons in Cholistan sand are mostly derived from Punjabi tributaries (~69%), with the remaining ~31% supplied by the Upper Indus sources (i.e., Karakorum-Hindukush, Ladakh-Kohistan, and Nanga Parbat). In contrast, zircons in Sindh sand are derived more from Upper Indus sources (~54%; Fig. 9a) than from Punjabi tributaries (~46%), with notably higher contributions from the Kohistan Arc (~10% *vs*. only ~2% in Cholistan) and Nanga Parbat Massif (~8% *vs*. ~3% in Cholistan) (Table 3; Fig. 9b).

East et al. (2015) argued that eolian sand in the southern Thar Desert was largely blown from the Indus Delta. The comparison with detrital zircons from modern Lower Indus River sand (Clift et al., 2004; Fig. 9c) indicates a greater supply from Punjabi tributaries (~38% *vs*. ~17% for Sindh Desert sand) at the expense of Karakorum and Kohistan. Detrital zircons from Indus deltaic sand dated as ~7 ka (sample TH-10 in Clift et al., 2008; Fig. 9d, e), however, appear to be dominantly derived from the Karakoram (~65%), implying drastic provenance changes in the Lower Indus occurred after 7 ka. Zircon ages from sand deposited at ~14 ka (sample KB-40 in Clift et al., 2008; Fig. 9f) more closely match zircon ages in Sindh sand, but with an inferred greater contribution from Ladakh-Kohistan arcs (~27% *vs.* ~10%) and a much lower contribution from Punjabi tributaries (~16% *vs.* ~46%).

The comparison between zircon ages in Cholistan Desert and modern Lower Indus River sands indicate a similar contribution from Punjabi tributaries. Cholistan dunes have a similar signature as Marot borehole samples 6 and 12 (Clift et al., 2012; Fig. 9g, h), although a more important zircon supply from Punjabi tributaries is indicated for the Sutlej River for Marot-6 dated as ~7 ka, and for the Beas River for Marot-12 dated as > 49 ka (Table 3).

7.3. Summary of provenance results

The combination of petrographic, heavy-mineral, and detrital-geochronology methods allow us to put firm constraints on the provenance of Thar Desert sands, indicating that eolian dunes in the northern Cholistan area were largely fed by Punjabi tributaries sourced in the Himalayan belt (primarily the Sutlej-Beas River system, with potential additional contributions from the now extinct Ghaggar-Hakra paleo-river). Instead, eolian dunes in the southern Sindh area have more similar composition as Indus Delta sands and were largely supplied by the Lower Indus River.

The concentration of heavy minerals in the sediment varies depending on the supply from contrasting source units, and thus varies between different tributaries with unique bedrock exposures in their headwaters. There are examples where sediments appear to have been partially eroded from source areas that are not present upstream of the sampling location in the adjacent river system. For example, in northern Cholistan it might not be expected to see sediment eroded from Nanga Parbat, Ladakh-Kohistan or the Karakorum. Although the percentage of heavy minerals from those areas is less than other parts of the desert the values are not zero and require recycling via aeolian transport from the south. It should also be remembered that different source areas may have contrasting degrees of fertility in the different heavy minerals, so that the proportion of sediment derived from each source and calculated from heavy mineral percentages may not be representative of the total mass flux. Hydraulic sorting is a crucial factor for the concentration and variety of heavy minerals from which we derive provenance information. Compared to the modern Upper Indus and Thal Desert sands, Cholistan Desert sand is notably poorer in quartz and sedimentary to low-rank metasedimentary rock fragments. Cholistan sediments are however richer in feldspars, volcanic, metavolcanic and metabasic rock fragments, heavy minerals and especially hypersthene, documenting a significantly greater relative contribution from the Kohistan arc.

We can explore the provenance of the desert dunes further using the *DZStats* program from Saylor and Sundell (2016) (Appendix A Table A7). In this approach, a series of samples are directly compared with one another using a statistical test, in this case the Kuiper Test to quantify their similarity. We compare the Sindh and Cholistan dune averages with potential sources, i.e., the Upper Indus at Attock, the modern delta at Thatta, two post-LGM delta samples (TH-10 at ~7 ka and KB-40 at ~14 ka), together with the modern Sutlej and two older fluvial channel sands from Marot (Marot-6 at ~7 ka and Marot-12 >49 ka). These sands are from the Ghaggar-Hakra. There is no direct measurement of what the Sutlej or other Punjabi tributaries looked like during the Mid Holocene or older times. The results are shown in Figure 10 and Table 4. No strict affinity, however, is observed between the dune fields and either modern Upper Indus or Sutlej River sands. The compositional signatures of Sindh dunes are closest to deltaic sediments dated between ~7 and 14 ka, whereas those of Cholistan dunes are closest to samples 6 and 12 from the Marot borehole, dated as ~7 and > 49 ka (Clift et al., 2012). We conclude that eolian sands accumulated in the Thar Desert largely before ~7 ka, most plausibly during the early Holocene when summer monsoon winds were at a maximum (Gupta et al., 2003).

8. Climatic changes associated with the Asian Monsoon

8.1. Aeolian sedimentation since the Last Glacial Maximum

A chronology of the evolution of the Thar Desert based on TL dating of aeolian sediments (Singhvi et al., 2010) revealed multiple phases of dune accretion since 200 ka, interrupted by hiatuses associated with precession-driven climate. In the eastern Thar Desert, the last major phase of dune growth started between 17 ka and 14 ka and lasted until 9 ka, at the onset of the early Holocene wet stage (Dhir et al., 2010, 2012; Singhvi et al., 2010; Garzanti et al., 2020b). During this time, the region experienced a transitional climate, with southwesterly monsoon winds strengthened after the LGM, characterized by a weak summer monsoon. Mesolithic artifacts dated to the first millennium of the Holocene have been found on top of sand dunes in both eastern Thar and Thal deserts, suggesting similar accretion histories (Biagi et al., 2019). In contrast, the western Thar Desert (subject of this study) was supplied with sediment since the beginning of the wetter early Holocene and expanded further westward as the climate dried after the mid-Holocene (East et al., 2015).

The incision of moraines and fluvial terraces in the high Karakorum, Kohistan, and Himalayan mountains led to increased sediment fluxes during the deglaciation period that followed the LGM (Blöthe et al., 2014; Garzanti et al., 2020b; Clift and Jonell, 2021). During the LGM and early deglacial period, summer monsoon rains were weak but meltwater fluxes from shrinking mountain glaciers were high, and sediment was carried to the lower reaches and delta, and accumulated on the northern floodplains (Saini et al., 2009; Giosan et al., 2012). As monsoon rains strengthened in the Early Holocene, fluvial sediment fluxes increased but sedimentation became focused in the lower reaches and delta through the Holocene, whereas incision prevailed in the northern floodplains after 10 ka (Giosan et al., 2012). Floodplain and deltaic sediments were deflated by summer monsoonal winds and blown throughout the

Holocene into the western Thar Desert but mostly only from 17 to 9 ka in the eastern Thar Desert (East et al., 2015; Singhvi et al., 2010).

8.2. Paleoclimatic effects of the Asian Monsoon

The intensity of the Asian Monsoon varies over long as well as millennial and even shorter timescales (Clemens and Prell, 2003; Jonell et al., 2018). The Quaternary period experienced significant variations in monsoon intensity, which were influenced by insolation maxima and the export of latent heat from the ocean (Clemens et al., 1991; Clark et al., 2006; Caley et al., 2011). The relationship between monsoon intensity and orbital forcing is strong, but with a delayed response. Thar Desert climate in the Holocene was highly sensitive to changes in Asian Monsoon strength, as evidenced by the presence of an extinct river in the Cholistan Desert and of related fluvial deposition in the Ghaggar-Hakra River upstream (Oldham, 1886; Durcan, 2012; Alok et al., 2023). Relative aridity during the LGM (23–20 ka) was followed by an increase in monsoon intensity in the early Holocene (Durcan, 2012; Fleitmann et al., 2003), and enhanced regional precipitation led to incision of the Sutlej River into the flood plains after 10 ka. Wet conditions associated with strong winds favored sediment supply, deflation, and rapid accumulation in the central Thar Desert through most of the Holocene (Singhvi et al., 2010; Chatterjee and Ray, 2017). Around 4.5 ka, monsoonal rains and consequently fluvial activity in the Ghaggar-Hakra River weakened (Durcan et al., 2019), and along western edge of the desert dunes started to advance over the floodplain (East et al., 2015; Durcan et al., 2019).

9. Conclusions

This study employs an integrated provenance approach, combining bulk petrography, heavy minerals, and detrital zircon dating to constrain the origin of sediments in the western

Thar Desert. Eolian dunes consist of feldspatho-litho-quartzose metamorphiclastic sand in the northern Cholistan region and of litho-feldspatho-quartzose sedimentaclastic sand in the southern Sindh region. The quartz/feldspar ratio is much higher in Cholistan sand, largely supplied by Punjabi tributaries sourced in the Himalayan belt (chiefly the Sutlej-Beas River system), than for Sindh sand showing notably closer affinity with Lower Indus River sand. This is confirmed by heavy-mineral suites, which contain notably higher percentages of green to brown amphibole in Sindh dunes than in Cholistan dunes. U-Pb age signatures of detrital-zircons are not equally distinct, with slightly more Neoproterozoic to Paleozoic ages recorded in Sindh than in Cholistan. Young zircons yielding Cretaceous to Miocene ages shed by Ladakh-Kohistan arc and Karakorum batholiths occur both in Cholistan and Sindh, indicating extensive mixing of zircon grains originally derived from the Upper Indus but likely transported into the desert from the lower reaches and delta by monsoon winds.

Compositional affinities between Thar Desert dunes and sand presently transported by the modern Indus and Sutlej rivers are limited. Conversely, Sindh dunes are closest to Indus Delta sediments dated between ~7 and 14 ka, whereas Cholistan dunes are closest to samples from the Marot borehole in Cholistan dated as ~7 and > 49 ka. We thus infer that eolian sand largely accumulated before ~7 ka, most plausibly during the wet and windy early Holocene stage, when both sediment supply and summer monsoon winds reached maximum and sand transport into the Thar Desert was thus particularly efficient.

Acknowledgments

The senior author would like to thank the PhD program of the Department of Earth and Environmental Sciences of Milano Bicocca University for supporting his research and the International Association of Sedimentology for receiving a postgraduate grant for detrital-zircon dating. The Charles T. McCord Jr Chair in Petroleum Geology at LSU supported some of this research.

SUPPLEMENTARY MATERIALS

Supplementary data associated with this article, to be found in the online version at http://dx.doi.____________, include information on sampling sites (Table A1), together with the complete datasets on sand petrography (Table A2), heavy minerals (Table A3), original and literature data on U-Pb zircon-age distributions (Table A4), percentages of U-Pb zircon-age distributions in diverse source-rock domains (Table A5), *DZMix* results summary (Table A6), and *DZStats* input dataset (Table A7). The Google-Earth™ map of sampling sites Thar.kmz is also provided.

FIGURE and TABLE CAPTIONS

Figure 1. Geological map of the western Himalaya syntaxis and other ranges drained by the Indus River system, showing the major tectonic blocks of these regions which form the primary sources of sediment to the Indus River modified after Garzanti et al. (2020). Location of modern sand samples from both Thar Desert and Indus drainage system are shown.

Figure 2. Satellite image of Pakistan and adjacent regions (from Google Earth™). Figure shows sampling locations for desert sand and modern rivers. Note the distribution of the sediments collected during this study in Cholistan and further south in eastern Sindh. Original image from Google Earth. Location of modern sand samples from both Thar Desert and Indus drainage system are shown.

Figure 3. Photomicrographs of representative sediment samples from both Sindh and Cholistan deserts. Grains appear slightly more angular in Sindh sand. Q = Quartz, P = plagioclase, K = K-feldspar, Ls = sedimentary lithic, Lms = metamorphic lithic, c = carbonate, Amp = amphibole, Ep = Epidote.

Figure 4. Petrography of Thar Desert sand compared with sand from potential source regions. A) QFL diagram (compositional fields after Garzanti, 2019); B) QFP diagram; C) Ls-Lm-Lv diagram (Ingersoll et al., 1984). Note greater affinity of Cholistan sand with Punjab tributaries sourced in the Himalayan belt and of Sindh sand with Indus River sand. D) Heavy mineral discrimination diagram (Morton et al., 1999). E) Principal component plot (Vermeesch et al., 2016). Data from contributing sediment sources from Garzanti et al. (2020). Q = quartz; F = feldspars (P = plagioclase; KF = K-feldspar); L = lithic fragments (Lm = metamorphic; Ls =

sedimentary) Amp = amphibole; Ep = epidote: Grt = garnet; Ky = kyanite; Px = pyroxene; Sill = sillimanite; St = staurolite.

Figure 5. Detrital-zircon geochronology of five studied samples compared with literature data from potential sources. Left and center panels: KDE diagrams for U-Pb age spectra in modern fluvial and eolian sands from the Indus catchment. Four pie diagrams to the right compare age signatures of Lower Indus and Punjabi tributaries with eolian sands of Cholistan and Sindh.

Figure 6. Multidimensional Scale (MDS) diagram comparing U-Pb age spectra of detrital zircons in Cholistan and Sindh dunes with potential sources.

Figure 7. U-Pb age spectra of detrital zircon in the studied Thar Desert samples plotted as KDE and compared with potential sources throughout the Indus catchment. Data sources cited in text.

Figure 8. Pie diagrams depict the results of provenance budgets obtained by forward mixing calculations based on heavy-mineral assemblages. A) Lower Indus; B) Upper Indus; C) Sindh dunes with tectonic domains as end members; D) Cholistan dunes with tectonic domains as end members; E) Sindh dunes with rivers as end members; F) Cholistan dunes with rivers as end members. Data sources from Garzanti et al. (2005, 2020).

Figure 9. Pie diagrams depict the results of provenance budgets based on detrital zircon U-Pb spectra and estimated using *DZMix* software (Sundell and Saylor, 2017; plots based on V factor of Kuiper test, full results provided in Appendix Table A5). A) Sindh zircons; B) Cholistan zircons. C) Upper Indus zircons (Alizai et al., 2011; Clift et al., 2022). D) Lower Indus zircons

(Clift et al., 2004). E, F) Indus delta at 7 ka and 14 ka (Clift et al., 2008). G, H) Paleo-Ghaggar-Hakra channel at 7 ka and <49 ka (Marot borehole; Clift et al., 2012). Data on desert sands from East et al. (2015) are included. Note greater zircon contribution from Punjabi tributaries sourced in the Himalayan belt in Cholistan than in Sindh.

Figure 10. Heat map (blue = similar; red = dissimilar) comparing U-Pb zircon signatures of Thar Desert sands with selected fluvial samples (as determined by K-S testing using the *DZStats* program of Saylor and Sundell, 2016; details provided in Appendix Table A5). Note affinities between modern Cholistan dunes with Marot channel sands older than 7 ka, and between modern Sindh dunes with Indus Delta sediments older than 7 ka.

Table 1. Petrography and heavy minerals composition of Thar (Cholistan and Sindh) Desert sand carried by the Indus River and Punjabi tributaries from the different NW Himalayan sources. Q = quartz; F = feldspars (KF = K-feldspar; P = plagioclase; L = lithic grains (Lvm = volcanic and metavolcanic; Lc = carbonate and metacarbonate; Lh = chert; Lsm = shale, siltstone, slate, and metasiltstone; Lmf = felsic metamorphic; Lmb = metabasite; Lu = ultramafic); HM = heavy minerals; MI* = Metamorphic Index; tHMC = transparent heavy-mineral concentration. ZTR = zircon + tourmaline + rutile; Ttn = titanite; Ep = epidote-group minerals; Grt = garnet; SKS = staurolite + kyanite + sillimanite; Amp = amphibole; Px = pyroxene (Cpx = clinopyroxene; Opx = orthopyroxene, mostly hypersthene); & tHM = other transparent heavy minerals (apatite, chloritoid, Cr-spinel, olivine, prehnite, pumpellyite, brookite, andalusite, baryte).

Table 2. An average age structure of the zircon U-Pb ages from Sindh and Cholistan, together with the lower Indus and an average of all the Punjabi tributaries. *Italic:* for standard deviations.

Table 3. (a). The contribution of the heavy minerals into the Indus (Lower and Upper) River and Thar (Cholistan and Sindh) Desert from different NW Himalaya sources. (b). Sediments supply as heavy minerals into the Lower Indus and Thar (Cholistan and Sindh) from the Punjabi tributaries.

Table 4. Detrital Zircon contribution in percentages in the Thar (Sindh and Cholistan) Desert and Indus River with NW Himalayas and Punjabi tributaries

REFRENCES

Ahmad, F., 2008. Runoff farming in reducing rural poverty in Cholistan desert. Sociedade & Natureza, 20, pp.177-188.

Ahmad, F., 2011. Soil classification and micromorphology: A case study of Cholistan Desert. Journal of Soil Science and Environmental Management, 2(11), pp.321-329.

Akbar, G., Khan, T.N. and Arshad, M., 1996. Cholistan Desert, Pakistan. Rangelands, 18, 124-128.

Akhter, R. and Arshad, M., 2006. Arid rangelands in the Cholistan desert (Pakistan). Science et changements planétaires/Sécheresse, 17(1), pp.210-217.

Alizai, A., Carter, A., Clift, P.D., VanLaningham, S., Williams, J.C. and Kumar, R., 2011a. Sediment provenance, reworking and transport processes in the Indus River by U–Pb dating of detrital zircon grains. Global and Planetary Change, 76(1-2), pp.33-55.

Alizai, A., Clift, P.D., Giosan, L., VanLaningham, S., Hinton, R., Tabrez, A.R., Danish, M. and Facility, T.E.I.M., 2011b. Pb isotopic variability in the modern-Pleistocene Indus River system measured by ion microprobe in detrital K-feldspar grains. Geochimica et Cosmochimica Acta, 75(17), pp.4771-4795.

Alizai, A., Clift, P.D. and Still, J., 2016. Indus Basin sediment provenance constrained using garnet geochemistry. Journal of Asian Earth Sciences, 126, pp.29-57.

Alok, A., Pant, N.C., Das, K., Tsutsumi, Y., Petrie, C.A., Kumar, P., Chopra, S., Saini, H.S. and Khan, A.A., 2023. New insights into the geological evolution of palaeorivers and their relationship to the Indus Civilization and Early Historic settlements on the plains of Haryana, NW India. Geological Society, London, Special Publications, 515(1), pp.233-249.

Amundson, R., Pendall, E. and Meadow, R.H., 1986. Pedology and Late Quaternary environments surrounding Harappa: a review and synthesis. Harappa excavations, 1990, pp.13-27.

Andò, S., 2020. Gravimetric separation of heavy minerals in sediments and rocks. Minerals, 10(3), p.273.

Belnap, J., Munson, S.M. and Field, J.P., 2011. Aeolian and fluvial processes in dryland regions: the need for integrated studies. Ecohydrology, 4(5), pp.615-622.

Biagi, P., Starnini, E. and Ghauri, Z.S., 2020. Mahi Wala 1 (MW-1): a Mesolithic site in the Thal desert of Punjab (Pakistan). Asian Archaeology, 3(1-2), pp.1-8.

Blöthe, J.H. and Korup, O., 2013. Millennial lag times in the Himalayan sediment routing system. Earth and Planetary Science Letters, 382, pp.38-46.

Bookhagen, B. 2010. Appearance of extreme monsoonal rainfall events and their impact on erosion in the Himalaya. Geomatics, Natural Hazards and Risk, 1(1), 37-50.

Bullard, J.E. and Livingstone, I., 2002. Interactions between aeolian and fluvial systems in dryland environments. Area, 34(1), pp.8-16.

Bullard, J.E. and McTainsh, G.H., 2003. Aeolian-fluvial interactions in dryland environments: examples, concepts and Australia case study. Progress in Physical Geography, 27(4), pp.471-501.

Bracken, L.J., Turnbull, L., Wainwright, J. and Bogaart, P., 2015. Sediment connectivity: a framework for understanding sediment transfer at multiple scales. Earth Surface Processes and Landforms, 40(2), pp.177-188.

Blinkhorn, J., 2014. Late Middle Palaeolithic surface sites occurring on dated sediment formations in the Thar Desert. Quaternary International, 350, pp.94-104.

Blinkhorn, J., Achyuthan, H., Jaiswal, M. and Singh, A.K., 2020. The first dated evidence for Middle-Late Pleistocene fluvial activity in the central Thar Desert. Quaternary Science Reviews, 250, p.106656.

Boos, W.R. and Kuang, Z., 2010. Dominant control of the South Asian monsoon by orographic insulation versus plateau heating. Nature, 463(7278), pp.218-222.

Chatterjee, A. and Ray, J.S., 2017. Sources and depositional pathways of mid-Holocene sediments in the Great Rann of Kachchh, India: Implications for fluvial scenario during the Harappan Culture. Quaternary International, 443, pp.177-187.

Chauhan, S.S., 2003. Desertification control and management of land degradation in the Thar desert of India. Environmentalist, 23, pp.219-227.

Clemens, S.C. and Prell, W.L., 2003. A 350,000 year summer-monsoon multi-proxy stack from the Owen Ridge, Northern Arabian Sea. Marine Geology, 201(1-3), pp.35-51.

Clemens, S., Prell, W., Murray, D., Shimmield, G. and Weedon, G., 1991. Forcing mechanisms of the Indian Ocean monsoon. Nature, 353(6346), pp.720-725.

Clift, P.D. and Jonell, T.N., 2021. Monsoon controls on sediment generation and transport: Mass budget and provenance constraints from the Indus River catchment, delta and submarine fan over tectonic and multimillennial timescales. Earth-Science Reviews, 220, p.103682.

Clift, P.D., Shimizu, N., Layne, G.D., Blusztajn, J.S., Gaedicke, C., Schluter, H.U., Clark, M.K. and Amjad, S., 2001. Development of the Indus Fan and its significance for the erosional history of the Western Himalaya and Karakoram. Geological Society of America Bulletin, 113(8), pp.1039-1051.

Clift, P.D., Lee, J.I., Hildebrand, P., Shimizu, N., Layne, G.D., Blusztajn, J., Blum, J.D., Garzanti, E. and Khan, A.A., 2002. Nd and Pb isotope variability in the Indus River System: implications for sediment provenance and crustal heterogeneity in the Western Himalaya. Earth and Planetary Science Letters, 200(1-2), pp.91-106.

Clift, P.D., Campbell, I.H., Pringle, M.S., Carter, A., Zhang, X., Hodges, K.V., Khan, A.A. and Allen, C.M., 2004. Thermochronology of the modern Indus River bedload: New insight into the controls on the marine stratigraphic record. Tectonics, 23(5).

Clift, P.D., Giosan, L., Blusztajn, J., Campbell, I.H., Allen, C., Pringle, M., Tabrez, A.R., Danish, M., Rabbani, M.M., Alizai, A. and Carter, A., 2008. Holocene erosion of the Lesser Himalaya triggered by intensified summer monsoon. Geology, 36(1), pp.79-82.

Clift, P.D., Carter, A., Giosan, L., Durcan, J., Duller, G.A., Macklin, M.G., Alizai, A., Tabrez, A.R., Danish, M., VanLaningham, S. and Fuller, D.Q., 2012. U-Pb zircon dating evidence for a Pleistocene Sarasvati River and capture of the Yamuna River. Geology, 40(3), pp.211-214.

Clift, P.D., Mark, C., Alizai, A., Khan, H. and Jan, M.Q., 2022. Detrital U–Pb rutile and zircon data show Indus River sediment dominantly eroded from East Karakoram, not Nanga Parbat. Earth and Planetary Science Letters, 600, p.117873.

Crawford, M.B. and Searle, M.P., 1992. Field relationships and geochemistry of pre-collisional (India-Asia) granitoid magmatism in the central Karakoram, northern Pakistan. Tectonophysics, 206(1-2), pp.171-192.

Caley, T., Malaizé, B., Zaragosi, S., Rossignol, L., Bourget, J., Eynaud, F., Martinez, P., Giraudeau, J., Charlier, K. and Ellouz-Zimmermann, N., 2011. New Arabian Sea records help decipher orbital timing of Indo-Asian monsoon. Earth and Planetary Science Letters, 308(3-4), pp.433-444.

Clark, P.U., Archer, D., Pollard, D., Blum, J.D., Rial, J.A., Brovkin, V., Mix, A.C., Pisias, N.G. and Roy, M., 2006. The middle Pleistocene transition: characteristics, mechanisms, and implications for long-term changes in atmospheric pCO2. Quaternary Science Reviews, 25(23-24), pp.3150-3184.

Critelli, S. and Ingersoll, R.V., 1994. Sandstone petrology and provenance of the Siwalik Group (northwestern Pakistan and western-southeastern Nepal). Journal of Sedimentary Research, 64(4a), pp.815-823.

Comas-Cufí, M. and Thió I Fernández de Henestrosa, S., 2011, May. CoDaPack 2.0: a stand-alone, multi-platform compositional software. In © International Workshop on Compositional Data Analysis (4th: 2011: Sant Feliu de GuÍxols, Girona). CODAWORK 2011: International Workshop on Compositional Data Analysis, hold on May 9-13rd. 2011, Sant Feliu de Guíxols, Girona. Universitat Politècnica de Catalunya. Centre Internacional de Mètodes Numèrics en Enginyeria (CIMNE).

Dhir, R.P., Singhvi, A.K., Andrews, J.E., Kar, A., Sareen, B.K., Tandon, S.K., Kailath, A. and Thomas, J.V., 2010. Multiple episodes of aggradation and calcrete formation in Late Quaternary aeolian sands, Central Thar Desert, Rajasthan, India. Journal of Asian Earth Sciences, 37(1), pp.10-16.

Dhir, R.P. and Singhvi, A.K., 2012. The Thar Desert and its antiquity. Current Science, pp.1001-1008.

Debon, F., Le Fort, P., Dautel, D., Sonet, J. and Zimmermann, J.L., 1987. Granites of western Karakorum and northern Kohistan (Pakistan): a composite Mid-Cretaceous to upper Cenozoic magmatism. Lithos, 20(1), pp.19-40.

Durcan, J.A., Roberts, H.M., Duller, G.A.T. and Alizai, A.H., 2010. Testing the use of range-finder OSL dating to inform field sampling and laboratory processing strategies. Quaternary Geochronology, 5(2-3), pp.86-90.

Durcan, J.A., 2012. Luminescence dating of sediments in Punjab, Pakistan: implications for the collapse of the Harappan Civilisation (Doctoral dissertation, Aberystwyth University).

Durcan, J.A., Thomas, D.S., Gupta, S., Pawar, V., Singh, R.N. and Petrie, C.A., 2019. Holocene landscape dynamics in the Ghaggar-Hakra palaeochannel region at the northern edge of the Thar Desert, northwest India. Quaternary International, 501, pp.317-327.

East, A.E., Clift, P.D., Carter, A., Alizai, A. and VanLaningham, S., 2015. Fluvial–eolian interactions in sediment routing and sedimentary signal buffering: an example from the Indus Basin and Thar Desert. Journal of Sedimentary Research, 85(6), pp.715-728.

El-Baz, F., 1983. A geological perspective of the desert. In Origin and Evolution of Deserts. S. G. Wells and D. R. Haragan (Eds.), University of New Mexico Press, Albuquerque, pp. 163–83.

Feder, A., Zimmermann, R., Stollhofen, H., Caracciolo, L., Garzanti, E. and Andreani, L., 2018. Fluvial-aeolian sedimentary facies, sossusvlei, namib desert. Journal of Maps, 14(2), pp.630-643.

Fleitmann, D., Burns, S.J., Mudelsee, M., Neff, U., Kramers, J., Mangini, A., Matter, A., 2003. Holocene forcing of the Indian monsoon recorded in a stalagmite from southern Oman. Science, 300(5626): 1737-1739.

Gabriel, K.R., 1971. The biplot graphic display of matrices with application to principal component analysis. Biometrika, 58(3), pp.453-467.

Garzanti, E., 2017. The maturity myth in sedimentology and provenance analysis. Journal of Sedimentary Research, 87(4), pp.353-365.

Garzanti, E., 2019a. The Himalayan Foreland Basin from collision onset to the present: A sedimentary–petrology perspective. Geological Society, London, Special Publications, 483(1), pp.65-122.

Garzanti, E., 2019b. Petrographic classification of sand and sandstone. Earth-Science Reviews, 192, pp.545-563.

Garzanti, E., and Andò, S., 2007. Plate tectonics and heavy mineral suites of modern sands. Developments in Sedimentology, 58, pp.741-763.

Garzanti, E. and Andò, S., 2019. Heavy minerals for junior woodchucks. Minerals, 9(3), p.148.

Garzanti, E. and Vezzoli, G., 2003. A classification of metamorphic grains in sands based on their composition and grade. Journal of Sedimentary Research, 73(5), pp.830-837.

Garzanti, E. and Van Haver, T., 1988. The Indus clastics: forearc basin sedimentation in the Ladakh Himalaya (India). Sedimentary Geology, 59(3-4), pp.237-249.

Garzanti, E., Critelli, S. and Ingersoll, R.V., 1996. Paleogeographic and paleotectonic evolution of the Himalayan Range as reflected by detrital modes of Tertiary sandstones and modern sands (Indus transect, India and Pakistan). Geological society of america bulletin, 108(6), pp.631-642.

Garzanti, E., Vezzoli, G., Andò, S., Paparella, P. and Clift, P.D., 2005. Petrology of Indus River sands: a key to interpret erosion history of the Western Himalayan Syntaxis. Earth and Planetary Science Letters, 229(3-4), pp.287-302.

Garzanti, E., Resentini, A., Vezzoli, G., Andò, S., Malusà, M. and Padoan, M., 2012. Forward compositional modelling of Alpine orogenic sediments. Sedimentary Geology, 280, pp.149-164.

Garzanti, E., Vermeesch, P., Al-Ramadan, K.A., Andò, S., Limonta, M., Rittner, M. and Vezzoli, G., 2017. Tracing Transcontinental Sand Transport: from Anatolia–zagros To the Rub'Al Khali Sand Sea. Journal of Sedimentary Research, 87(11), pp.1196-1213.

Garzanti, E., Vermeesch, P., Rittner, M. and Simmons, M., 2018. The zircon story of the Nile: Time- structure maps of source rocks and discontinuous propagation of detrital signals. Basin Research, 30(6), pp.1098-1117.

Garzanti, E., Andò, S. and Vezzoli, G., 2020a. Provenance of Cenozoic Indus Fan sediments (IODP Sites U1456 and U1457). Journal of Sedimentary Research, 90(9), pp.1114-1127.

Garzanti, E., Liang, W., Andò, S., Clift, P.D., Resentini, A., Vermeesch, P. and Vezzoli, G., 2020b. Provenance of Thal Desert sand: Focused erosion in the western Himalayan syntaxis and foreland-basin deposition driven by latest Quaternary climate change. Earth-science reviews, 207, p.103220.

Garzanti, E., Pastore, G., Stone, A., Vainer, S., Vermeesch, P. and Resentini, A., 2022. Provenance of Kalahari Sand: Paleoweathering and recycling in a linked fluvial-aeolian system. Earth-Science Reviews, 224, p.103867.

Gábris, G. and Nádor, A., 2007. Long-term fluvial archives in Hungary: response of the Danube and Tisza rivers to tectonic movements and climatic changes during the Quaternary: a review and new synthesis. Quaternary Science Reviews, 26(22-24), pp.2758-2782.

Glennie, K.W., Singhvi, A.K., Lancaster, N. and Teller, J.T., 2002. Quaternary climatic changes over southern Arabia and the Thar Desert, India. Geological Society, London, Special Publications, 195(1), pp.301-316.

Guillot, S., Garzanti, E., Baratoux, D., Marquer, D., Mahéo, G. and de Sigoyer, J., 2003. Reconstructing the total shortening history of the NW Himalaya. Geochemistry, Geophysics, Geosystems, 4(7).

Gupta, A.K., Anderson, D.M., Overpeck, J.T., 2003. Abrupt changes in the Asian southwest monsoon during the Holocene and their links to the North Atlantic Ocean. Nature, 421: 354–356.

Giosan, L., Clift, P.D., Macklin, M.G., Fuller, D.Q., Constantinescu, S., Durcan, J.A., Stevens, T., Duller, G.A., Tabrez, A.R., Gangal, K. and Adhikari, R., 2012. Fluvial landscapes of the Harappan civilization. Proceedings of the National Academy of Sciences, 109(26), pp.E1688-E1694.

Griffin, W.L., 2008. GLITTER: data reduction software for laser ablation ICP-MS. Laser Ablation ICP-MS in the Earth Sciences: Current practices and outstanding issues, pp.308-311.

Haughton, P.D.W., Todd, S.P. and Morton, A.C., 1991. Sedimentary provenance studies. Geological Society, London, Special Publications, 57(1), pp.1-11.

Henderson, A.L., Najman, Y., Parrish, R., BouDagher‐ Fadel, M., Barford, D., Garzanti, E. and Andò, S., 2010. Geology of the Cenozoic Indus Basin sedimentary rocks: Paleoenvironmental interpretation of sedimentation from the western Himalaya during the early phases of India‐ Eurasia collision. Tectonics, 29(6).

Hu, X., Garzanti, E., Moore, T. and Raffi, I., 2015. Direct stratigraphic dating of India-Asia collision onset at the Selandian (middle Paleocene, 59±1 Ma). Geology, 43(10), pp.859-862.

Hubert, J.F., 1962. A zircon-tourmaline-rutile maturity index and the interdependence of the composition of heavy mineral assemblages with the gross composition and texture of sandstones. Journal of Sedimentary Research, 32(3), pp.440-450.

Ingersoll, R.V., Bullard, T.F., Ford, R.L., Grimm, J.P., Pickle, J.D. and Sares, S.W., 1984. The effect of grain size on detrital modes: a test of the Gazzi-Dickinson point-counting method. Journal of Sedimentary Research, 54(1), pp.103-116.

Jain, A.K. and Banerjee, D.M., 2020. The Indian subcontinent: its tectonics. Proceedings of the Indian National Science Academy, 86, pp.775-875.

Jackson, S. E., Pearson, N. J., Griffin, W. L., & Belousova, E. A. (2004). The application of laser ablation-inductively coupled plasma-mass spectrometry to in situ U–Pb zircon geochronology. Chem. Geol., 211(1-2), 47-69.

Jonell, T.N., Carter, A., Böning, P., Pahnke, K. and Clift, P.D., 2017. Climatic and glacial impact on erosion patterns and sediment provenance in the Himalayan rain shadow, Zanskar River, NW India. Bulletin, 129(7-8), pp.820-836.

Jonell, T.N., Owen, L.A., Carter, A., Schwenniger, J.L. and Clift, P.D., 2018. Quantifying episodic erosion and transient storage on the western margin of the Tibetan Plateau, upper Indus River. Quaternary Research, 89(1), pp.281-306.

Kar, A., 2013. Quaternary geomorphic processes and landform development in the Thar Desert of Rajasthan. Landforms Process. Environ. Manag, pp.225-256.

Kazmi, A.H., 1984. Geology of the Indus delta. Marine geology and oceanography of Arabian Sea and coastal Pakistan, pp.71-84.

Kruskal, J.B., Wish, M., 1978. Multidimensional scaling. Sage Publications, Newbury Park (CA), Quantitative applications in the social sciences. Sage Univer. Paper Ser. 07-011, 92.

Kumari, D., Prajapat, G., Goyal, S. and Agrawal, A., 2023. Modification of desert sand to soil using polymers for its agricultural potential. Journal of Arid Environments, 209, p.104899.

Langford, R.P., 1989. Fluvial- aeolian interactions: Part I, modern systems. Sedimentology, 36(6), pp.1023-1035.

Lee, J.I., Clift, P.D., Layne, G., Blum, J. and Khan, A.A., 2003. Sediment flux in the modern Indus River inferred from the trace element composition of detrital amphibole grains. Sedimentary Geology, 160(1-3), pp.243-257.

Lemennicier, Y., Le Fort, P., Lombardo, B., Pêcher, A. and Rolfo, F., 1996. Tectonometamorphic evolution of the central Karakorum (Baltistan, northern Pakistan). Tectonophysics, 260(1-3), pp.119-143.

Liang, W., Garzanti, E., Andò, S., Gentile, P. and Resentini, A., 2019. Multimineral fingerprinting of Transhimalayan and Himalayan sources of Indus-derived Thal Desert sand (central Pakistan). Minerals, 9(8), p.457.

Liang, W., Hu, X., Garzanti, E., Dong, X. and Zhang, Y., 2023. Fluvial- aeolian interaction and compositional variability in the river- fed Yarlung Tsangpo dune system (southern Tibet). Journal of Geophysical Research: Earth Surface, p.e2022JF006920.

Ludwig, K.R., 1998. On the treatment of concordant uranium-lead ages. Geochimica et Cosmochimica Acta, 62(4), pp.665-676.

Mange, M.A., and Morton, A.C., 2007. Geochemistry of heavy minerals. In: Mange MA, Wright DT (eds) Heavy Minerals in Use. Developments in Sedimentology 58. Elsevier, Amsterdam, pp 345-391.

Morton, A.C. and Hallsworth, C.R., 1999. Processes controlling the composition of heavy mineral assemblages in sandstones. Sedimentary geology, 124(1-4), pp.3-29.

Mughal, M.R. 1997. Ancient Cholistan - Archaeology and Architecture. Ferozsons (Pvt.) Ltd., Lahore. pp. 21.

Mughal, M.R., Iqbal, F., Afzal, M. and Hassan, M., 1996. Archaeological sites and monuments in Punjab: Preliminary results of explorations, 1992–96. Pa. Archaeol, 29, pp.1-474.

Najman, Y., Garzanti, E., Pringle, M., Bickle, M., Stix, J. and Khan, I., 2003. Early-Middle Miocene paleodrainage and tectonics in the Pakistan Himalaya. Geological Society of America Bulletin, 115(10), pp.1265-1277.

Najman, Y., Jenks, D., Godin, L., Boudagher-Fadel, M., Millar, I., Garzanti, E., Horstwood, M. and Bracciali, L., 2017. The Tethyan Himalayan detrital record shows that India–Asia terminal collision occurred by 54 Ma in the Western Himalaya. Earth and Planetary Science Letters, 459, pp.301-310.

Nordstrom, K.F., 2014. Living with shore protection structures: a review. Estuarine, coastal and shelf science, 150, pp.11-23.

Oldham, R.D., 1999. On probable changes in the geography of the Punjab and its rivers-An historico-geographical study. Memoirs-Geological Society of India, pp.81-88.

Petter, A.L., Steel, R.J., Mohrig, D., Kim, W. and Carvajal, C., 2013. Estimation of the paleoflux of terrestrial-derived solids across ancient basin margins using the stratigraphic record. Bulletin, 125(3-4), pp.578-593.

Prell, W.L., 1984. Variation of monsoonal upwelling: a response to changing solar radiation. Climate processes and climate sensitivity, 29, pp.48-57.

Prins, M.A., Zheng, H., Beets, K., Troelstra, S., Bacon, P., Kamerling, I., Wester, W., Konert, M., Huang, X., Ke, W. and Vandenberghe, J., 2009. Dust supply from river floodplains: the case of the lower Huang He (Yellow River) recorded in a loess–palaeosol sequence from the Mangshan Plateau. Journal of Quaternary Science: Published for the Quaternary Research Association, 24(1), pp.75-84.

Rahaman, W., Singh, S.K., Sinha, R. and Tandon, S.K., 2009. Climate control on erosion distribution over the Himalaya during the past~ 100 ka. Geology, 37(6), pp.559-562.

Ramsey, M.S., Christensen, P.R., Lancaster, N. and Howard, D.A., 1999. Identification of sand sources and transport pathways at the Kelso Dunes, California, using thermal infrared remote sensing. Geological Society of America Bulletin, 111(5), pp.646-662.

Resentini, A., Goren, L., Castelltort, S. and Garzanti, E., 2017. Partitioning sediment flux by provenance and tracing erosion patterns in Taiwan. Journal of Geophysical Research: Earth Surface, 122(7), pp.1430-1454.

Rolland, Y., Mahéo, G., Guillot, S. and Pêcher, A., 2001. Tectono- metamorphic evolution of the Karakorum Metamorphic complex (Dassu–Askole area, NE Pakistan): Exhumation of mid- crustal HT–MP gneisses in a convergent context. Journal of metamorphic Geology, 19(6), pp.717-737.

Rolland, Y., Pecher, A. and Picard, C., 2000. Middle Cretaceous back-arc formation and arc evolution along the Asian margin: the Shyok Suture Zone in northern Ladakh (NW Himalaya). Tectonophysics, 325(1-2), pp.145-173.

Roy, P.D. and Smykatz-Kloss, W., 2007. REE geochemistry of the recent playa sediments from the Thar Desert, India: an implication to playa sediment provenance. Geochemistry, 67(1), pp.55-68.

Saylor, J.E. and Sundell, K.E., 2016. Quantifying comparison of large detrital geochronology data sets. Geosphere, 12(1), pp.203-220.

Sláma, J., Košler, J., Condon, D.J., Crowley, J.L., Gerdes, A., Hanchar, J.M., Horstwood, M.S., Morris, G.A., Nasdala, L., Norberg, N. and Schaltegger, U., 2008. Plešovice zircon—a new natural reference material for U–Pb and Hf isotopic microanalysis. Chemical Geology, 249(1-2), pp.1-35.

Saini, H.S., Tandon, S.K., Mujtaba, S.A.I., Pant, N.C. and Khorana, R.K., 2009. Reconstruction of buried channel-floodplain systems of the northwestern Haryana Plains and their relation to the'Vedic'Saraswati. Current Science, 97(11), pp.1634-1643.

Sam, L., Gahlot, N. and Prusty, B.G., 2015. Estimation of dune celerity and sand flux in part of West Rajasthan, Gadra area of the Thar Desert using temporal remote sensing data. Arabian Journal of Geosciences, 8, pp.295-306.

Searle, M.P., Khan, M.A., Fraser, J.E., Gough, S.J. and Jan, M.Q., 1999. The tectonic evolution of the Kohistan‐ Karakoram collision belt along the Karakoram Highway transect, north Pakistan. Tectonics, 18(6), pp.929-949.

Singhvi, A.K. and Kar, A., 2004. The aeolian sedimentation record of the Thar Desert. Journal of Earth System Science, 113, pp.371-401.

Singhvi, A.K., Williams, M.A.J., Rajaguru, S.N., Misra, V.N., Chawla, S., Stokes, S., Chauhan, N., Francis, T., Ganjoo, R.K. and Humphreys, G.S., 2010. A∼ 200 ka record of climatic change and dune activity in the Thar Desert, India. Quaternary Science Reviews, 29(23-24), pp.3095-3105.

Singhvi, A.K., Kaushal, R.K. and Parida, S., 2022. Luminescence dating and Quaternary Geology: The Indian Narrative. Journal of the Palaeontological Society of India, 67(1), pp.183-210.

Sinha, R., Yadav, G.S., Gupta, S., Singh, A. and Lahiri, S.K., 2013. Geo-electric resistivity evidence for subsurface palaeochannel systems adjacent to Harappan sites in northwest India. Quaternary International, 308, pp.66-75.

Singh, A. and Sinha, R., 2019. Fluvial response to climate change inferred from sediment cores from the Ghaggar–Hakra paleochannel in NW Indo–Gangetic plains. Palaeogeography, Palaeoclimatology, Palaeoecology, 532, p.109247.

Searle, M.P., Parrish, R.R., Thow, A.V., Noble, S.R., Phillips, R.J. and Waters, D.J., 2010. Anatomy, age and evolution of a collisional mountain belt: the Baltoro granite batholith and Karakoram Metamorphic Complex, Pakistani Karakoram. Journal of the Geological Society, 167(1), pp.183-202.

Stein, A., 1942. A survey of ancient sites along the" lost" Sarasvati River. The Geographical Journal, 99(4), pp.173-182.

Srivastava, A., Thomas, D.S., Durcan, J.A. and Bailey, R.M., 2020. Holocene palaeoenvironmental changes in the Thar Desert: An integrated assessment incorporating new insights from aeolian systems. Quaternary Science Reviews, 233, p.106214.

Sundell, K.E. and Saylor, J.E., 2017. Unmixing detrital geochronology age distributions. Geochemistry, Geophysics, Geosystems, 18(8), pp.2872-2886.

Thomas, D.S. and Wiggs, G.F., 2008. Aeolian system responses to global change: challenges of scale, process and temporal integration. Earth Surface Processes and Landforms: The Journal of the British Geomorphological Research Group, 33(9), pp.1396-1418.

Thomas, P.J., Juyal, N., Kale, V.S. and Singhvi, A.K., 2007. Luminescence chronology of late Holocene extreme hydrological events in the upper Penner River basin, South India. Journal of Quaternary Science: Published for the Quaternary Research Association, 22(8), pp.747-753.

Trimble, S.W., 1983. A sediment budget for Coon Creek basin in the Driftless Area, Wisconsin, 1853-1977. American Journal of Science, 283(5), pp.454-474.

Treloar, P.J., Petterson, M.G., Jan, M.Q. and Sullivan, M.A., 1996. A re-evaluation of the stratigraphy and evolution of the Kohistan arc sequence, Pakistan Himalaya: implications for magmatic and tectonic arc-building processes. Journal of the Geological Society, 153(5), pp.681-693.

Valdiya, K.S., 2002, Saraswati: the river that Disappeared: Hyderabad, India, 1st University Press, 116 p.

van de Kamp, P.C. and Leake, B.E., 1985. Petrography and geochemistry of feldspathic and mafic sediments of the northeastern Pacific margin. Earth and Environmental Science Transactions of the Royal Society of Edinburgh, 76(4), pp.411-449.

Velbel, M.A. and Saad, M.K., 1991. Palaeoweathering or diagenesis as the principal modifier of sandstone framework composition? A case study from some Triassic rift-valley redbeds of eastern North America. Geological Society, London, Special Publications, 57(1), pp.91-99.

Vermeesch, P., 2013. Multi-sample comparison of detrital age distributions. Chemical Geology, 341, pp.140-146.

Vermeesch, P., 2018. IsoplotR: A free and open toolbox for geochronology. Geoscience Frontiers, 9(5), pp.1479-1493.

Vermeesch, P., 2021. On the treatment of discordant detrital zircon U–Pb data. Geochronology, 3(1), pp.247-257.

Vermeesch, P., Rittner, M., Petrou, E., Omma, J., Mattinson, C. and Garzanti, E., 2017. High throughput petrochronology and sedimentary provenance analysis by automated phase mapping and LAICPMS. Geochemistry, Geophysics, Geosystems, 18(11), pp.4096-4109.

Wang, B., Ding, Q., Fu, X., Kang, I.S., Jin, K., Shukla, J. and Doblas- Reyes, F., 2005. Fundamental challenge in simulation and prediction of summer monsoon rainfall. Geophysical Research Letters, 32(15).

Wasson, R.J., Smith, G.I. and Agrawal, D.P., 1984. Late Quaternary sediments, minerals, and inferred geochemical history of Didwana Lake, Thar Desert, India. Palaeogeography, palaeoclimatology, palaeoecology, 46(4), pp.345-372.

Whipple, K.X., 2001. Fluvial landscape response time: How plausible is steady-state denudation?. American Journal of Science, 301(4-5), pp.313-325.

Wright, R., Schuldenrein, J., Khan, M.A. and Mughal, M.R., 2005. The emergence of satellite communities along the Beas drainage: Preliminary results from Lahoma Lal Tibba and Chak Purbane Syal. In South Asia Archaeology 2001 (pp. 327-335). Editions Recherce sur les Civilisations-ADPF.

Wiedenbeck, M., Hanchar, J. M., Peck, W. H., Sylvester, P., Valley, J., Whitehouse, M., Kronz, A., Morishita, Y., Nasdala, L., Fiebig, J., Franchi, I., Girard, J.-P., Greenwood, R. C., Hinton, R., Kita, N., Mason, P. R. D., Norman, M., Ogasawara, M., Piccoli, P. M., … Zheng, Y.-F., 2004. Further Characterisation of the 91500 Zircon Crystal. Geostandards and Geoanalytical Research, 28(1), 9–39.

Zeitler, P.K., Chamberlain, C.P. and Smith, H.A., 1993. Synchronous anatexis, metamorphism, and rapid denudation at Nanga Parbat (Pakistan Himalaya). Geology, 21(4), pp.347-350.

Zhisheng, A., Clemens, S.C., Shen, J., Qiang, X., Jin, Z., Sun, Y., Prell, W.L., Luo, J., Wang, S., Xu, H. and Cai, Y., 2011. Glacial-interglacial Indian summer monsoon dynamics. science, 333(6043), pp.719-723.

Zhuang, G., Najman, Y., Tian, Y., Carter, A., Gemignani, L., Wijbrans, J., Jan, M.Q. and Khan, M.A., 2018. Insights into the evolution of the Hindu Kush–Kohistan–Karakoram from modern river sand detrital geo-and thermochronological studies. Journal of the Geological Society, 175(6), pp.934-948.

Figure 1 Click here to access/download;Figure;Figure 1. Geology Map.jpg

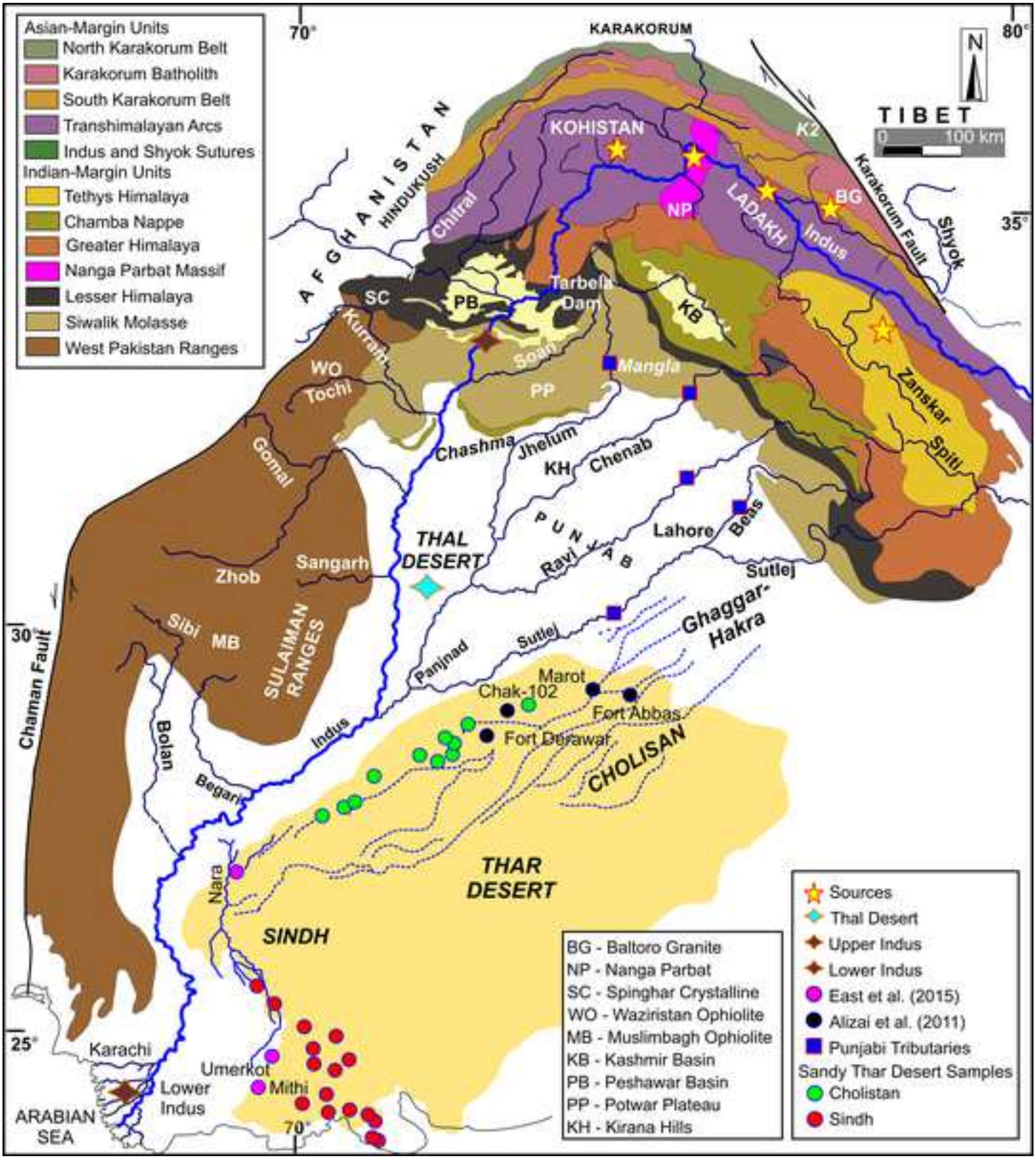

Figure 2

Click here to access/download;Figure;Figure 2. Setallite Map and River System.jpg

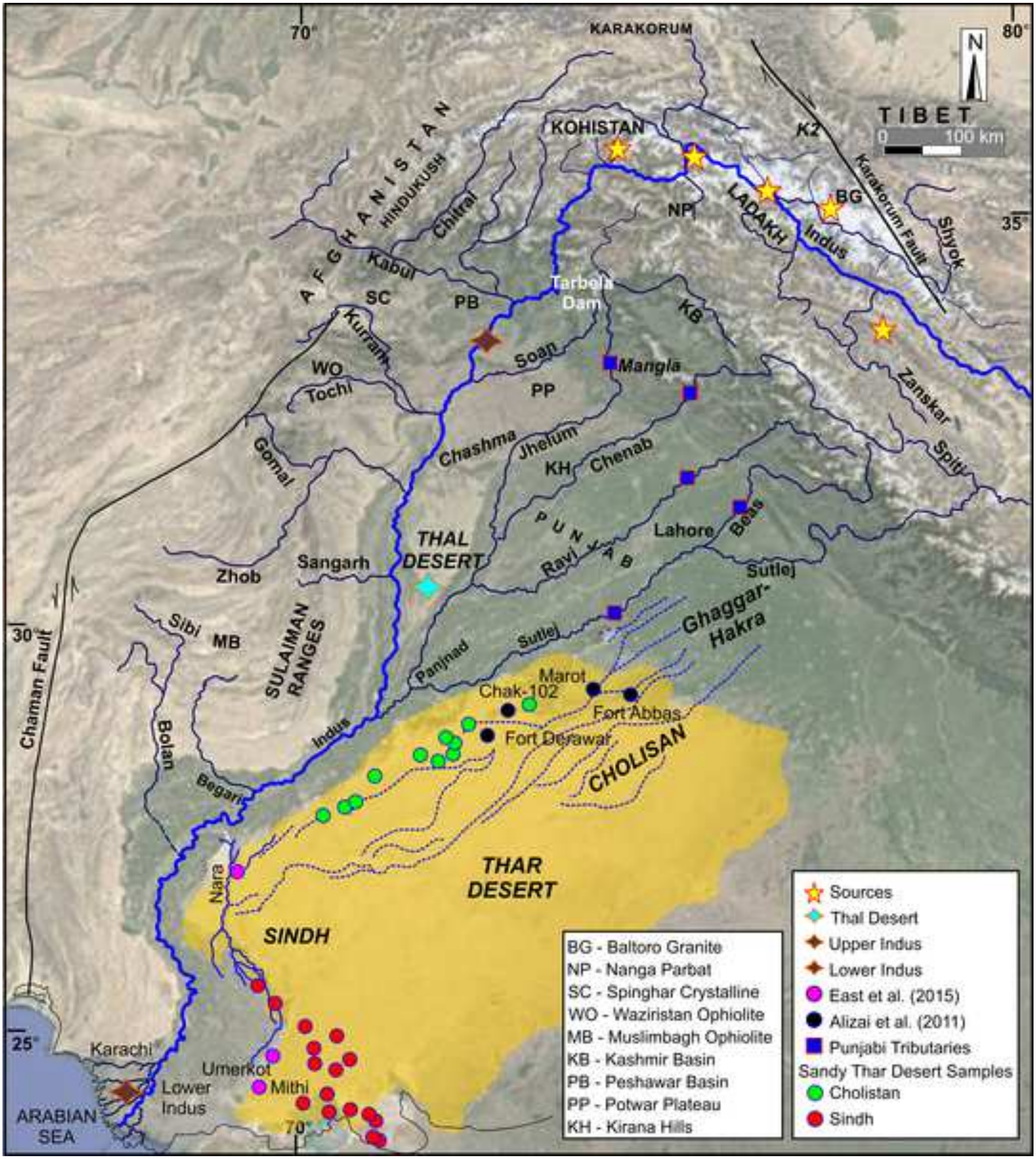

Figure 3

Click here to access/download;Figure;Figure 3. Thar Photo PT.jpg

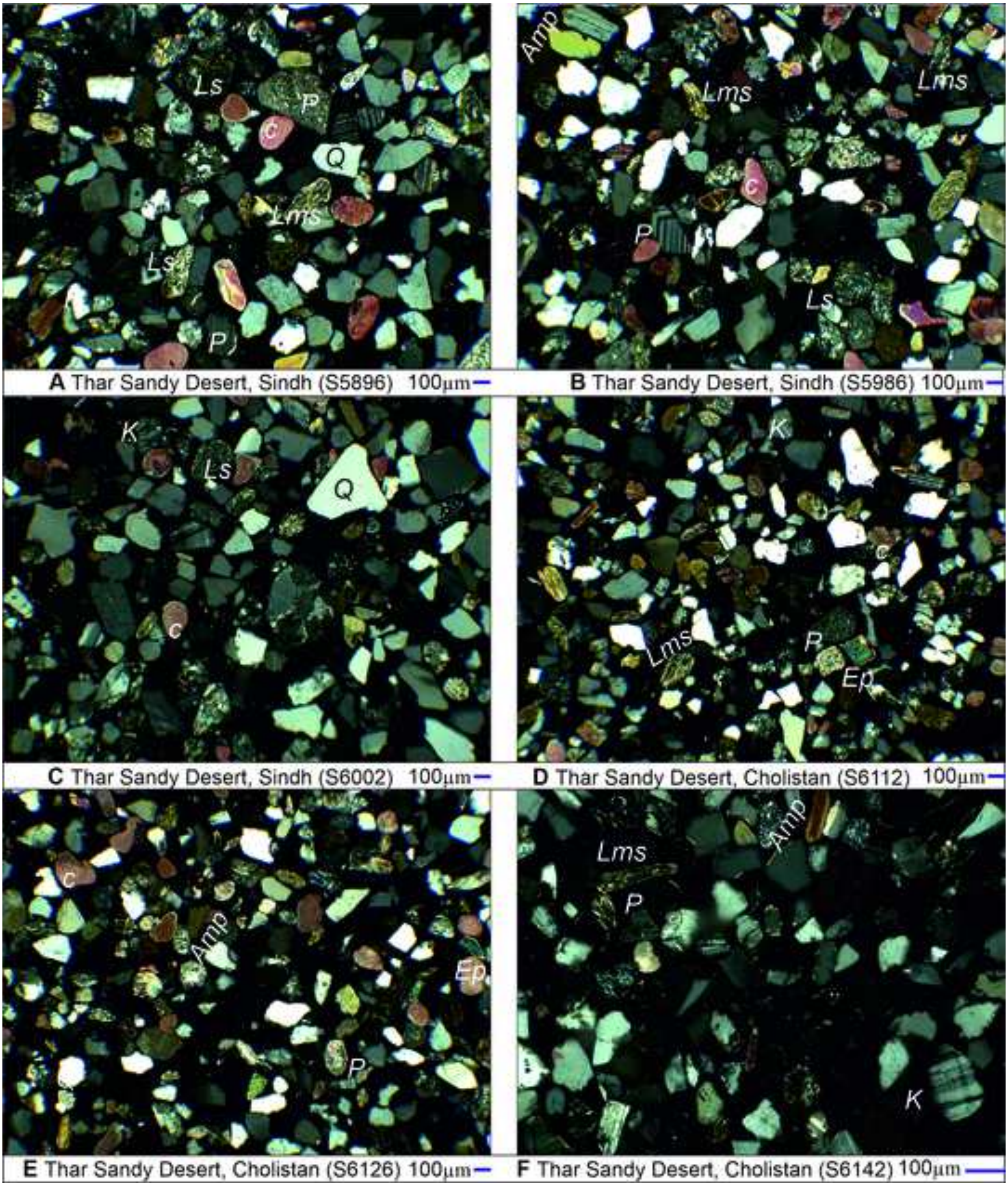

A Thar Sandy Desert, Sindh (S5896) 100μm

B Thar Sandy Desert, Sindh (S5986) 100μm

C Thar Sandy Desert, Sindh (S6002) 100μm

D Thar Sandy Desert, Cholistan (S6112) 100μm

E Thar Sandy Desert, Cholistan (S6126) 100μm

F Thar Sandy Desert, Cholistan (S6142) 100μm

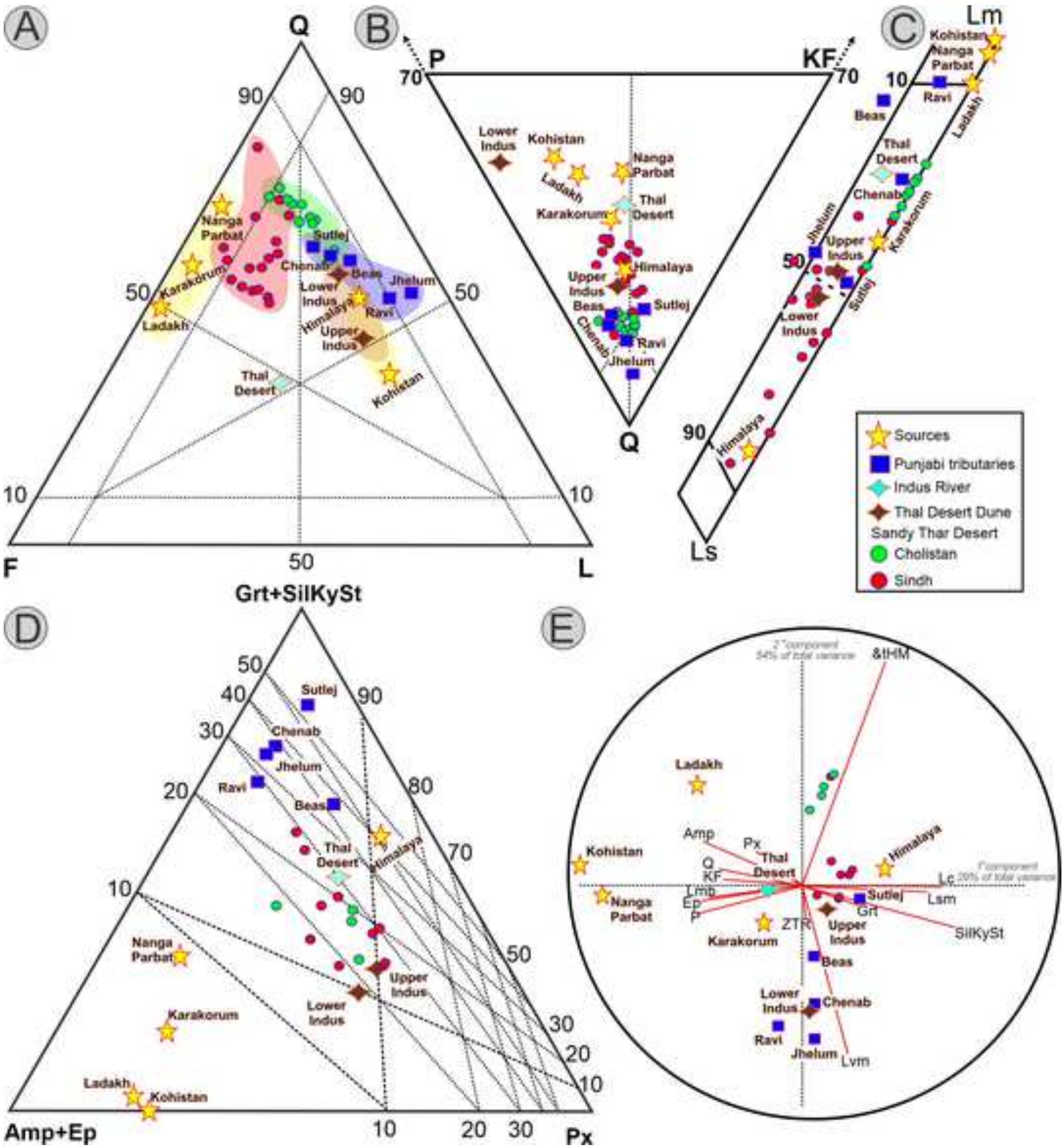
A
B
C
D
E
Q
F
L
P
KF
Lm
Ls
Grt+SilKySt
Amp+Ep
Px
Sources
Punjabi tributaries
Indus River
Thal Desert Dune
Sandy Thar Desert
Cholistan
Sindh
Kohistan
Nanga Parbat
Karakorum
Ladakh
Himalaya
Sutlej
Chenab
Beas
Jhelum
Ravi
Lower Indus
Upper Indus
Thal Desert
&tHM
Amp
Px
Q
KF
Lmb
Ep
P
ZTR
Grt
Lc
Lsm
SilKySt
Lvm

Figure 5

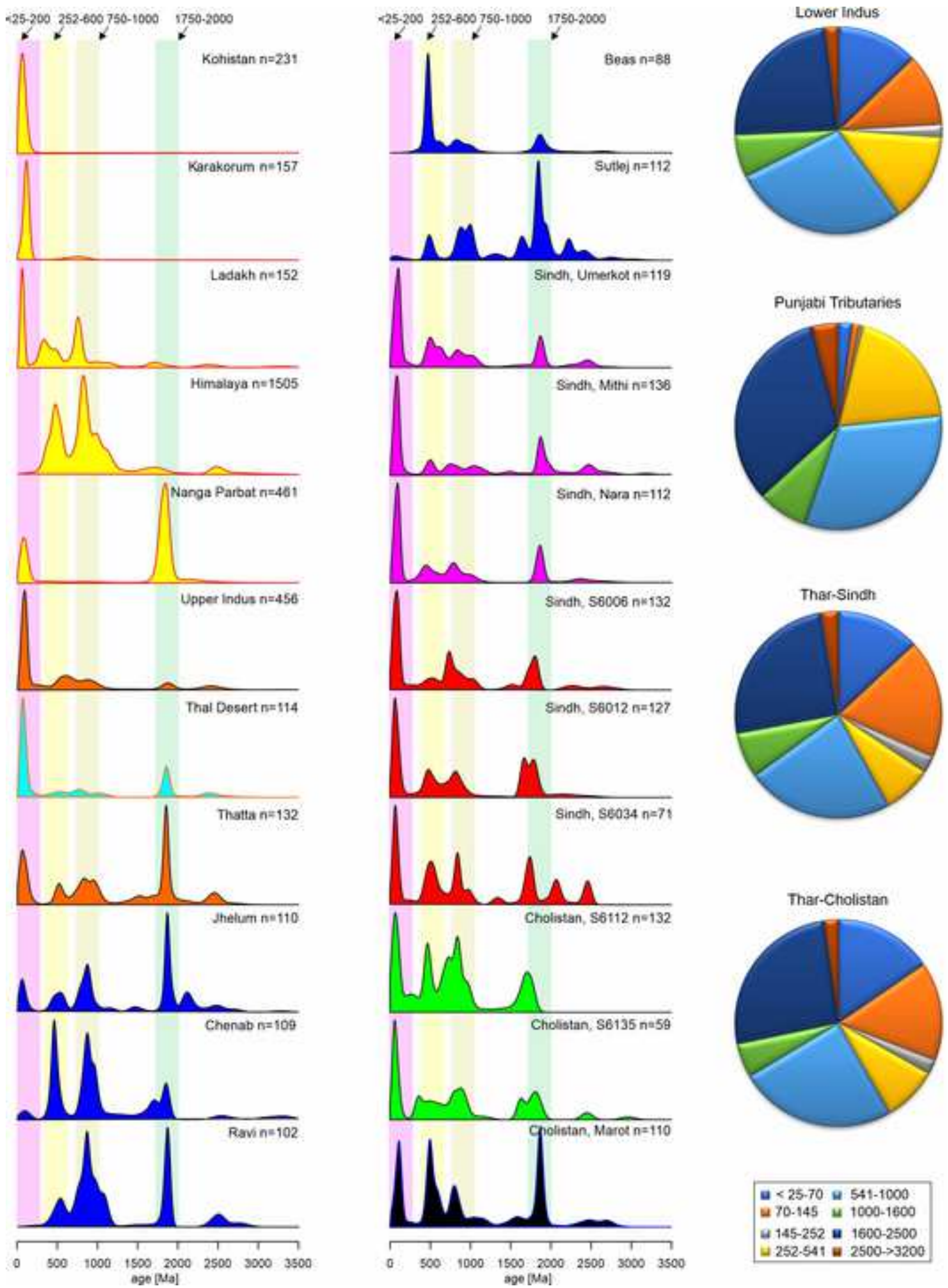

<25-200 252-600 750-1000 1750-2000
Kohistan n=231
Karakorum n=157
Ladakh n=152
Himalaya n=1505
Nanga Parbat n=461
Upper Indus n=456
Thal Desert n=114
Thatta n=132
Jhelum n=110
Chenab n=109
Ravi n=102
Beas n=88
Sutlej n=112
Sindh, Umerkot n=119
Sindh, Mithi n=136
Sindh, Nara n=112
Sindh, S6006 n=132
Sindh, S6012 n=127
Sindh, S6034 n=71
Cholistan, S6112 n=132
Cholistan, S6135 n=59
Cholistan, Marot n=110
0 500 1000 1500 2000 2500 3000 3500
age [Ma]
Lower Indus
Punjabi Tributaries
Thar-Sindh
Thar-Cholistan
< 25-70
70-145
145-252
252-541
541-1000
1000-1600
1600-2500
2500->3200

Figure 6

Click here to access/download;Figure;Figure 6. MDS.jpg

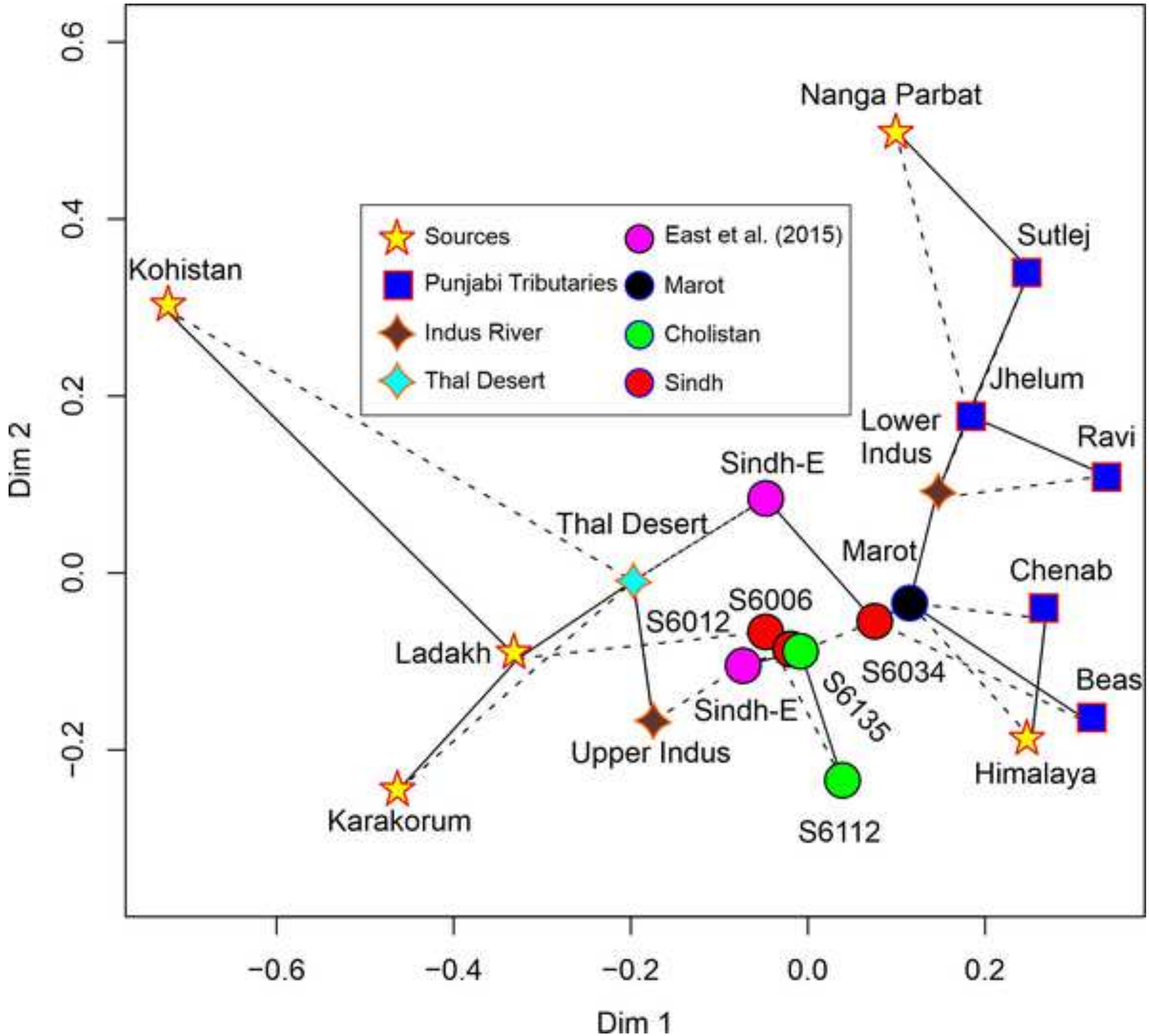

Figure 7

Click here to access/download;Figure;Figure 7. KDEs with Map.jpg

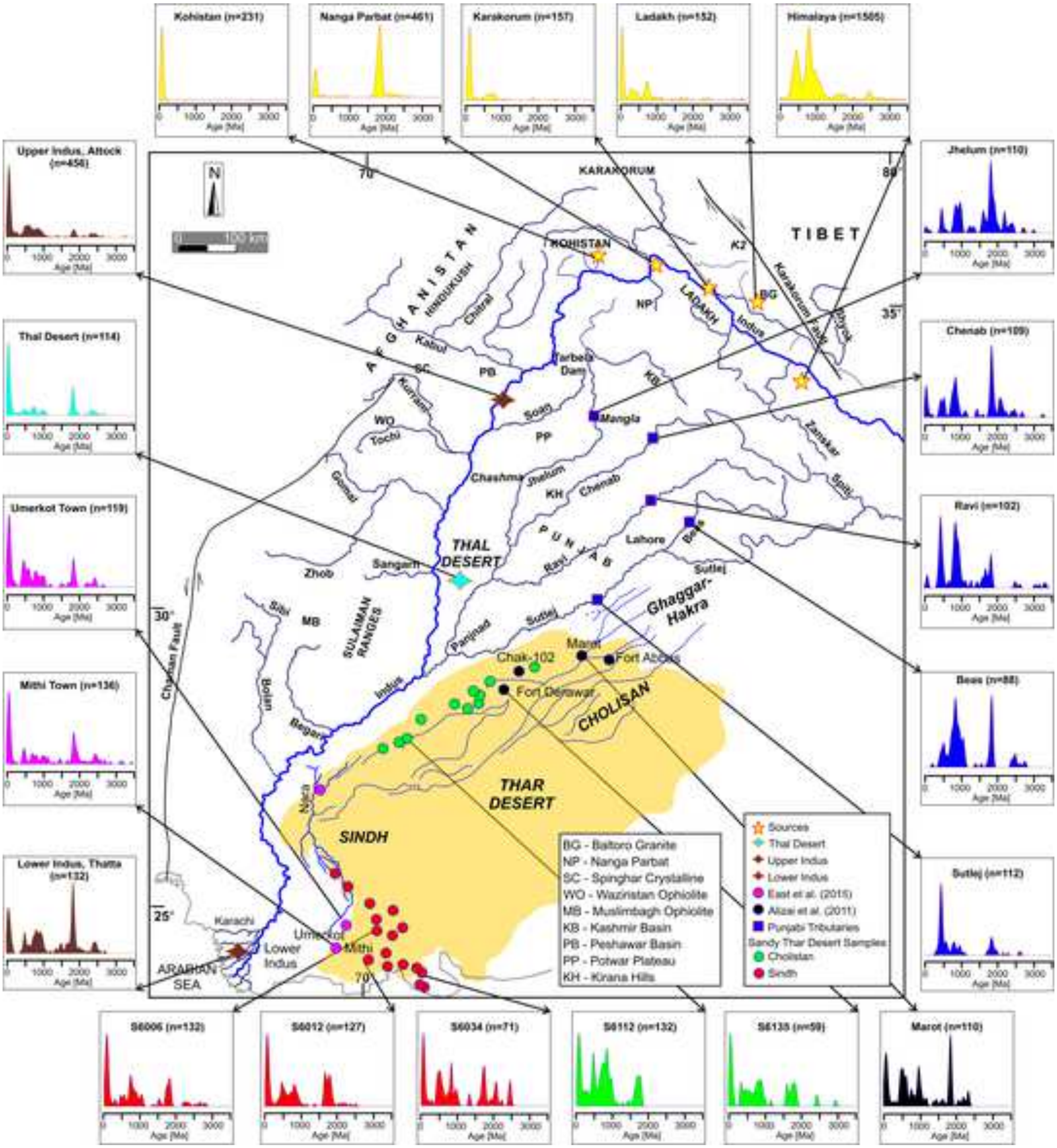

Figure 8

Click here to access/download;Figure;Figure 8. HM pie diagrams.jpg

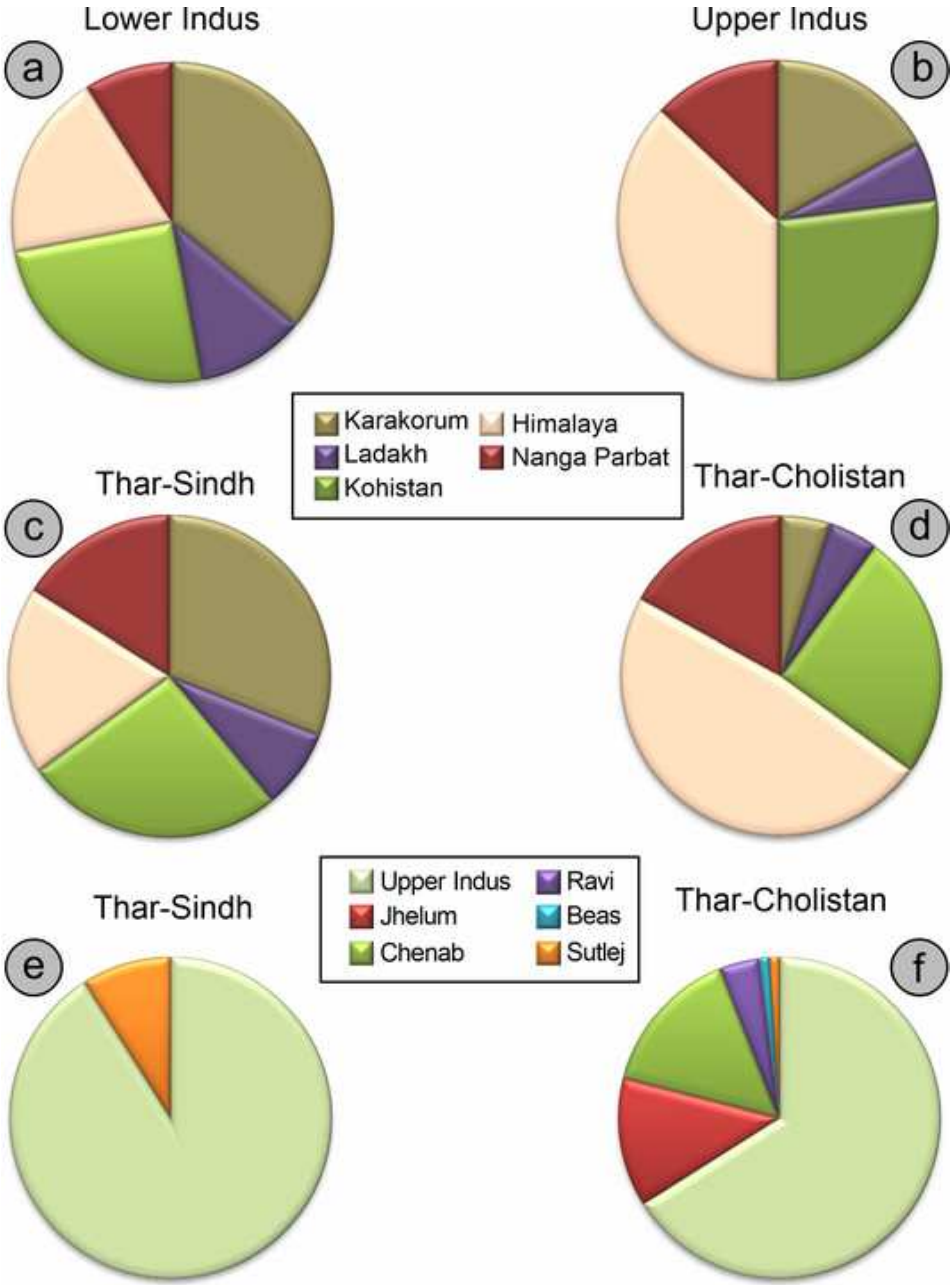

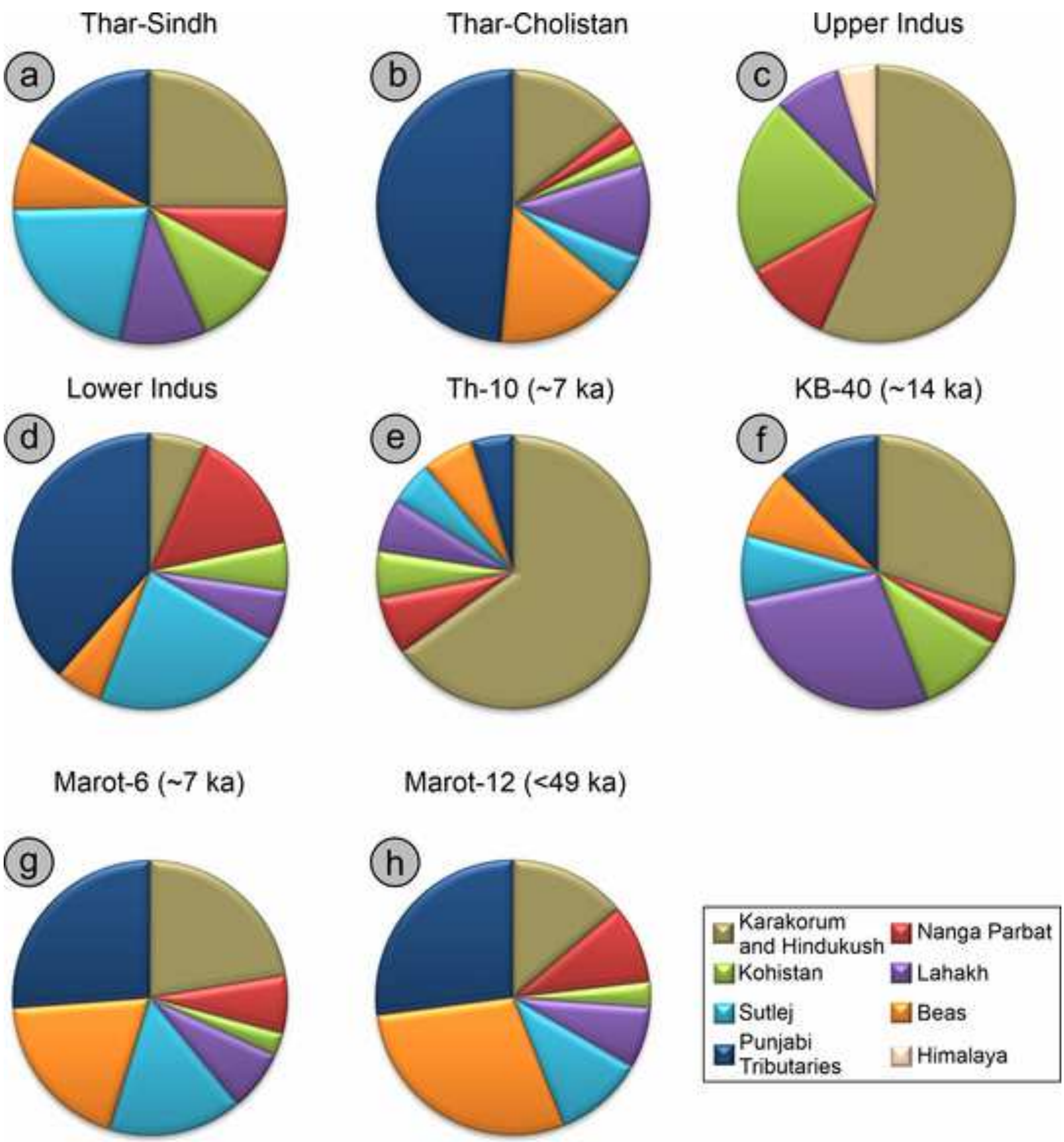

Thar-Sindh
a
Thar-Cholistan
b
Upper Indus
c
Lower Indus
d
Th-10 (~7 ka)
e
KB-40 (~14 ka)
f
Marot-6 (~7 ka)
g
Marot-12 (<49 ka)
h
Karakorum and Hindukush
Nanga Parbat
Kohistan
Lahakh
Sutlej
Beas
Punjabi Tributaries
Himalaya

Figure 10

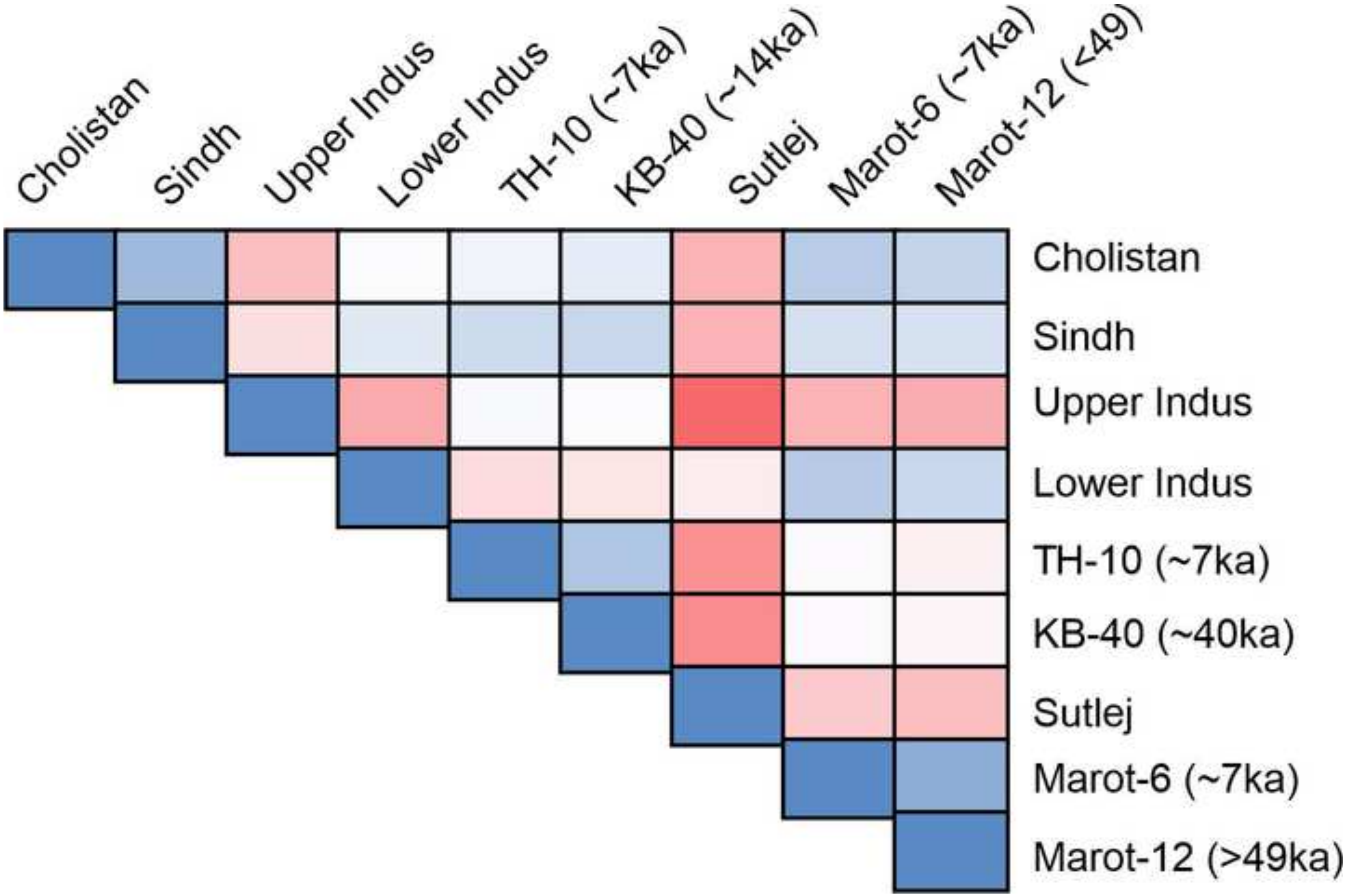
Cholistan
Sindh
Upper Indus
Lower Indus
TH-10 (~7ka)
KB-40 (~14ka)
Sutlej
Marot-6 (~7ka)
Marot-12 (<49)
Cholistan
Sindh
Upper Indus
Lower Indus
TH-10 (~7ka)
KB-40 (~40ka)
Sutlej
Marot-6 (~7ka)
Marot-12 (>49ka)

Table 1. minerals composition of Thar (Cholistan and Sindh) Desert sand carried by the Indus River and Punjabi tributaries from the different

River/Desert	Sample	Q	F	Lv	Lc	Lh	Lp	Lm	Lu	total	Qp/Q	P/F	MI*	tHMC	ZTR	Ttn	Ep	Grt	SKS	Amp	Cpx	Opx	&tHM	total
Thar Sindh We	**Average**	50	30	1	10	0	1	7	0	100.0	14	48	190	6	1	1	16	16	6	54	3	2	1	100.0
	Stand Dev	*0*	*0*	*1*	*1*	*0*	*0*	*1*	*0*		*7*	*2*	*22*	*1*	*1*	*1*	*3*	*0*	*3*	*5*	*2*	*0*	*0*	
Thar Sindh Cer	**Average**	58	27	1	6	0	2	6	0	100.0	10	58	161	5	2	0	15	13	2	59	6	2	1	100.0
	Stand Dev	*5*	*5*	*1*	*1*	*0*	*1*	*1*	*0*		*4*	*7*	*20*	*1*	*0*	*1*	*3*	*4*	*2*	*5*	*1*	*1*	*1*	
Thar Sindh Sou	**Average**	58	28	0	7	0	2	5	0	100.0	8	54	167	6	3	2	11	13	4	61	4	1	2	100.0
	Stand Dev	*5*	*5*	*0*	*3*	*0*	*0*	*2*	*0*		*2*	*9*	*17*	*3*	*3*	*2*	*1*	*4*	*1*	*3*	*1*	*1*	*1*	
Thar Cholistan	**Average**	62	17	0	7	0	1	13	0	100.0	5	50	268	15	3	2	26	9	6	44	4	4	2	100.0
	Stand Dev	*3*	*1*	*0*	*2*	*0*	*1*	*2*	*0*		*2*	*4*	*20*	*2*	*1*	*1*	*5*	*4*	*0*	*4*	*1*	*1*	*0*	
Thar Cholistan	**Average**	67	19	0	5	0	0	9	0	100.0	8	58	319	10	4	4	29	10	2	46	3	0	1	100.0
	Stand Dev	*1*	*2*	*0*	*1*	*0*	*1*	*1*	*0*		*3*	*5*	*13*											
Thar Cholistan	**Average**	67	18	0	6	0	0	9	0	100.0	8	51	309	11	2	2	19	10	6	50	5	2	3	100.0
	Stand Dev	*4*	*1*	*0*	*4*	*0*	*0*	*2*	*0*		*1*	*4*	*12*											
Thal	**S1462**	37	34	1	7	0	3	18	0	100.0	9	51	292	15	2	1	17	12	2	56	5	4	0	100.0
Sources																								
Karakorum	S1749	55	41	0	2	0	0	3	0	100.0	6	59	405	2	7	10	11	2	1	67	1	0	0	100.0
Ladakh	S4430	47	50	0	0	0	1	2	0	100.0	18	68	403	8	2	2	7	0	0	86	0	1	0	100.0
Kohistan	S1439	32	18	0	2	0	0	48	0	100.0	17	88	320	33	0	0	38	0	0	60	1	0	0	100.0
Swat-Kohistan	S1440	26	47	2	0	0	0	21	3	100.0	14	82	339	28	1	0	8	0	0	67	8	15	0	100.0
Himalaya	S4419	49	15	0	29	0	1	6	0	100.0	3	60	356	5	6	1	12	14	23	31	10	0	4	100.0
Nanga Parbat	S1432	67	30	0	0	0	0	3	0	100.0	18	50	390	17	1	0	19	7	0	71	1	0	0	100.0
Indus																								
Upper Indus	S1447/14	43	21	1	12	2	7	14	1	100.0	12	54	281	10	1	2	22	11	3	52	5	3	1	100.0
Lower Indus	S1489	53	17	1	12	1	5	11	0	100.0	5	54	364	9	2	1	17	6	3	61	6	2	0	100.0
Punjab tributaries																								
Jhelum	S1449	50	6	3	12	3	10	16	0	100.0	17	39	216	9	4	1	55	30	2	7	1	0	0	100.0
Chenab	S1450	58	16	0	5	0	8	13	0	100.0	8	42	261	1	2	0	31	19	16	30	1	0	0	100.0
Ravi	S1451	49	10	1	1	1	17	20	0	100.0	18	50	198	1	14	0	42	20	3	18	1	0	0	100.0
Sutlej	S1467	59	17	0	8	0	6	9	0	100.0	7	38	266	6	10	0	8	36	15	26	1	1	0	100.0
Beas	S2284	55	15	4	3	1	3	20	0	100.0	21	47	164	1	13	1	41	26	4	8	5	0	1	100.0

Q = quartz; F = feldspars (KF = K-feldspar; P = plagioclase; L = lithic grains (Lvm = volcanic and metavolcanic; Lc = carbonate and metacarbonate; Lh = chert; Lsm = shale, siltstone, slate, and metasiltstone; Lmf = felsic metamorphic; Lmb = metabasite; Lu = ultramafic); HM = heavy minerals; MI* = Metamorphic Index; tHMC = transparent heavy-mineral concentration. ZTR = zircon + tourmaline + rutile; Ttn = titanite; Ep = epidote-group minerals; Grt = garnet; SKS = staurolite + kyanite + sillimanite; Amp = amphibole; Px = pyroxene (Cpx = clinopyroxene; Opx = orthopyroxene, mostly hypersthene); & tHM = other transparent heavy minerals (apatite, chloritoid, Cr-spinel, olivine, prehnite, pumpellyite, brookite, andalusite,

Table 2 (Editable version)

Click here to access/download;Table (Editable version);Table 2. DZ_Population.xlsx

Table 2.	ucture of the zircon U-Pb ages from Sindh and Cholistan, together with the lower Indus and an average of all the												
	Era	Mioc	Dli/Eocer	Paleoc	Up-C	Lw-C	J	Tr	P	Neop	Mesop	Paleop	Arc
	Ages	<25	25-50	50-70	70-99	99-145	145-201	200-252	252-541	541-100(	.000-160	.600-250	500->3200
Cholistan	259	1.5%	8.9%	5.0%	5.4%	10.0%	1.2%	1.2%	8.5%	24.7%	5.3%	26.0%	2.3%
		0.0%	*0.3%*	*1.8%*	*3.1%*	*0.8%*	*0.6%*	*0.5%*	*3.5%*	*2.6%*	*4.2%*	*7.8%*	*2.1%*
Sindh	582	3.2%	3.9%	5.7%	3.4%	7.8%	1.5%	0.6%	13.8%	27.7%	6.7%	23.6%	2.1%
		0.3%	*1.2%*	*1.8%*	*1.8%*	*2.9%*	*0.4%*	*0.7%*	*2.3%*	*4.8%*	*1.8%*	*3.7%*	*1.7%*
Indus River	588	1.5%	4.8%	6.8%	7.6%	11.0%	1.8%	0.9%	7.6%	23.0%	7.1%	25.2%	2.7%
		1.1%	*2.5%*	*2.1%*	*8.5%*	*7.0%*	*0.7%*	*1.2%*	*2.2%*	*0.4%*	*3.9%*	*17.9%*	*0.4%*
Punj Trib	521	0.0%	1.3%	0.9%	0.5%	0.5%	0.2%	0.4%	19.5%	31.9%	7.9%	32.6%	4.2%
		0.0%	*2.0%*	*1.6%*	*0.8%*	*0.8%*	*0.4%*	*0.5%*	*17.9%*	*10.9%*	*4.1%*	*16.8%*	*1.9%*

Table 3 (Editable version)

Click here to access/download;Table (Editable version);Table 3. HM Supply_Thar.xlsx

Table 3a.	The contribution of the heavy minerals into the Indus (Lower and Upper) River and				
Sources	**Samples**	**Upper Indus**	**Lower Indus**	**Sindh**	**Cholistan**
Karakorum	S1749	17%	36%	31%	5%
Ladakh	S4430	6%	11%	8%	5%
Kohistan	S1440	27%	25%	26%	25%
Himalaya	S4419	37%	19%	19%	48%
Nanga Parbat	S1432	13%	9%	16%	17%

Table 3b.	Sediments supply as heavy minerals into the Lower Indus and Thar			
Sources	**Samples**	**Sindh**	**Cholistan**	**Lower Indus**
Lower Indus	Average	91%	66%	99%
Jhelum	S1449	0%	13%	0%
Chenab	S1450	0%	15%	0%
Ravi	S1451	0%	4%	0%
Beas	S2284	0%	1%	0%
Sutlej	S1467	9%	1%	1%

Table 4 (Editable version)

Click here to access/download;Table (Editable version);Table 4. DZ_Contribution.xlsx

Table 3.	Detrital Zircon contribution in percentages in the Thar (Sindh and Cholistan) Desert and Indus River with NW H								
Sources	**Sindh**	**TH-10 (7 ka**	**KB-40 (14 ka**	**Lower Indus**	**Cholistan**	**AROT-6 (7 k**	**ROT-12 (<49**	**Sources**	**Upper Indus**
Karakorum	25%	65%	30%	7%	15%	22%	14%	Karakorum	57%
Nanga Parb	8%	7%	3%	15%	3%	7%	9%	Nanga Parb	10%
Kohistan	10%	6%	10%	6%	3%	3%	3%	Kohistan	21%
Ladakh	10%	6%	28%	6%	11%	7%	7%	Ladakh	8%
Sutlej	21%	5%	8%	23%	5%	16%	11%	Zanskar	5%
Beas	8%	6%	8%	6%	15%	19%	29%		
Punjab Trib	17%	5%	12%	39%	49%	26%	27%		
Total Punja	**47%**	**16%**	**28%**	**67%**	**69%**	**61%**	**67%**		